Chapter I

Diluted magnetic semiconductor quantum dots

I.1   II-VI semiconductor quantum dots

I.1.1   Band structure of CdTe/ZnTe

ZnTe and CdTe are two II-VI semiconductor, meaning they are composed of an anion from the column VI of periodic table (Te), and a cation from the column II (Cd and Zn). They both crystallize as zinc blend when grown in Molecular Beam Epitaxy. As shown in Fig. I.1, in this structure, each species is organized in a face centred lattice, one them being shift from the other by a quarter of the [111] diagonal. Each ion is then in a tetragonal environment, meaning the zinc-blende structure is of the T_d space-group.

The external orbital of the cation are s for the cation ($4d^{10}5s^2$ for Cd, $3d^{10}4s^2$ for Zn) and p for the anion ($4d^{10}5s^25p^4$ for Te). Considering a N unit crystal, it then contain 8N valence electron, coming from the s and p levels of the ions. The s and p orbital of these atoms hybridize to form 8 levels, 4 bonding and 4 anti-bonding.

The lowest band of the bonding levels, coming from s orbitals, will be filled by 2N valence electron. 6N will be taken to fill the three higher energy bonding band, formed by the hybridization of p orbitals. Those bonding states form the valence band. At higher energy, the anti-bonding states form the conduction band. Since all the electron available are used to fill the valence band, the conduction band is empty in the ground state. The lower energy band of the conduction band are formed by the anti-symmetric combination of the s orbitals. At higher energy, the anti-symmetric hybridization of p orbitals form three other bands.

Introducing the spin-orbit interaction, the conduction band, formed by the hybridazation of s orbitals, is of Γ_6 (spherical) symmetry at the center of the
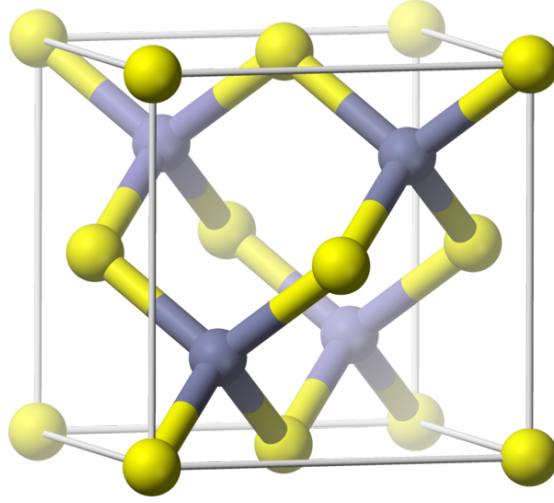
Figure I.1: Zinc-blende crystal elementary. Both CdTe and ZnTe crystallize in this structure.

Brillouin zone (for $k \simeq 0$), two-fold degenerated, with an orbital momentum (spin) $\sigma = 1/2$. In a similar fashion, the valence band will be split into to band: a first one of Γ_8 symmetry, with a spin $J = 3/2$, four-fold degenerated ; and the second one, at lower energy, of Γ_7 symmetry, with a spin $1/2$, two-fold degenerated. The splitting $\Gamma_7 - \Gamma_8$ is of $\Delta_{SO} \simeq 0.9$ eV in II-VI semiconductor.

The whole CdTe band structure is presented on Fig. I.2. One can note that CdTe is a direct gap semiconductor: the highest energy point of the valence band correspond to the lowest energy point of the conduction band, in Γ. As we move away from this point, the valence band into split two branches: the one with small curvature, meaning a high effective mass for the carriers on it, is called the heavy-hole (hh) band, while the one presenting the highest curvature and smallest effective mass is called the light-hole (lh) band.

One way to understand this evolution is to apply the **k.p** approximation, as proposed by Kane in 1957 [1]. This model gives an estimation of the electronic band structure starting from the exact solution and energy of the Schrödinger equation at the center of the Brillouin. The hamiltonian to resolve is then :

$$\left(\frac{p^2}{2m_0} + U(\mathbf{r}) \right) |\psi_{n,\mathbf{k}}\rangle = E_{n,\mathbf{k}} |\psi_{n,\mathbf{k}}\rangle \tag{I.1}$$

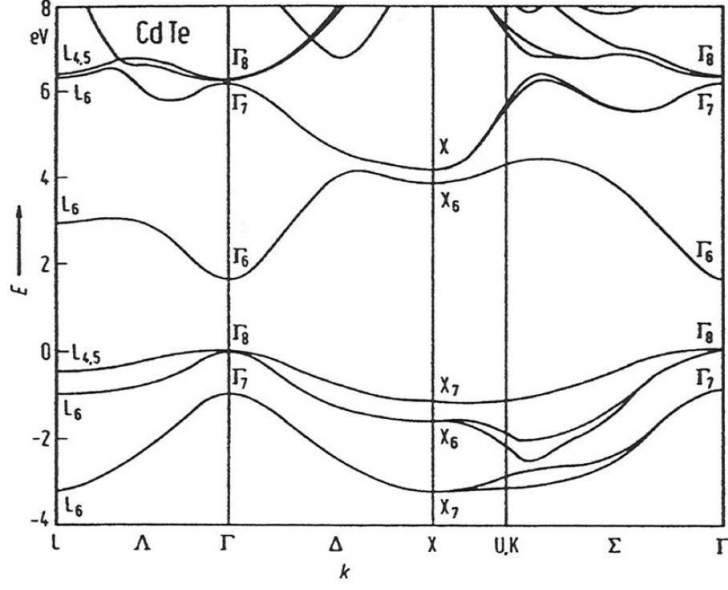with $U(\mathbf{r})$ the potential of the crystal and $|\psi_{n,\mathbf{k}}\rangle$ the Bloch wave, separated between

Figure I.2: CdTe band structure

a periodic part $u_{n,\mathbf{k}}(\mathbf{r})$ and plane-wave part $\exp(i\mathbf{k.r})$ as follow :

$$|\psi_{n,\mathbf{k}}\rangle = u_{n,\mathbf{k}}(\mathbf{r})\exp(i\mathbf{k.r}) \tag{I.2}$$

Neglecting the Γ_7 band at lower energy, we solve this hamiltonian for carrier on the Γ_6 and Γ_8 bands [2]. The z-axis is defined along the growth direction of the semiconductor and chosen as the quantization axis. The resolution was done in detail in Claire Le Gall PhD thesis [2]. We then find the energy:

$$
\begin{aligned}
E_c(k_z) &= E_c + \frac{\hbar^2 k_z^2}{2m_c}\\
E_{v,\pm\frac{1}{2}}(k_z) &= E_v - \frac{\hbar^2 k_z^2}{2m_{lh}}\\
E_{v,\pm\frac{3}{2}}(k_z) &= E_v + \frac{\hbar^2 k_z^2}{2m_0}
\end{aligned}
\tag{I.3}
$$

with E_c (respectively, E_v) the energy of the conduction band (respectively, the valence band), m_c the effective mass of the carrier on the conduction and m_{lh} the effective mass of the light hole. One can see that the splitting of the valence band separate the carrier with a spin $J_z = \pm\frac{3}{2}$ (hh) from the one with a spin $J_z = \pm\frac{1}{2}$ (lh). However, the neglecting of the bands other than Γ_6 and Γ_8 lead to a positive curvature for the hh. To correct this problem, we would have to take into

3

account higher energy conduction band, which will repel the hh band and give it its negative curvature.

Another solution to have the matrix describing the Γ_8 band is to use symmetry consideration. Luttinger showed in 1956 [3] that the only Hamiltonian fulfilling the cubic symmetry is:

$$\mathcal{H}_L = -\frac{h^2}{2m_0} \left(\gamma_1 k^2 I_4 - 2\gamma_2 \sum_i k_i^2 \left(J_i^2 - \frac{1}{3}J^2 \right) - 2\gamma_3 (k_x k_y (J_x J_y + J_y J_x) + c.p.) \right) \tag{I.4}$$

with γ_1, γ_2 and γ_3 the Luttinger parameters, I_4 the 4×4 identity matrix, $\mathbf{k}$ a vector of the Brillouin zone, $\mathbf{J}$ the orbital momentum operator with J_x, J_y and J_z being 4×4 matric satisfying $[J_x, J_y] = iJ_z$ and circular permutation, and $c.p$ standing for "circular permutation". This hamiltonian can be simplified using the parameters:

$$A = \gamma_1 + \frac{5}{2}\gamma_2$$
$$B = 2\gamma_2 \tag{I.5}$$
$$C = 2(\gamma_3 - \gamma_2)$$

The Luttinger hamiltonian can then be rewritten:

$$\mathcal{H}_L = -\frac{h^2}{2m_0} (Ak^2 I_4 - B(\mathbf{k}.\mathbf{J})^2 + C(k_x k_y (J_x J_y + J_y J_x) + c.p.)) \tag{I.6}$$

The B-term lift the degeneracy of the Γ_8 band into two sub-bands as shown above, and is invariant under arbitrary rotations. The C-term describes the warping of the valence band.

In the spherical approximation, the Luttinger hamiltonian has two eigenvalues:

$$E_{hh} = -\frac{\hbar^2 k^2}{2m_0(A - 2.25B)^{-1}} = -\frac{\hbar^2 k^2}{2m_0(\gamma_1 - 2\gamma_2)^{-1}} = -\frac{\hbar^2 k^2}{2m_{hh}}$$
$$E_{lh} = -\frac{\hbar^2 k^2}{2m_0(A - 0.25B)^{-1}} = -\frac{\hbar^2 k^2}{2m_0(\gamma_1 + 2\gamma_2)^{-1}} = -\frac{\hbar^2 k^2}{2m_{lh}} \tag{I.7}$$

We find then the value of the effective mass for the lh and for the hh. The hh band also presents here a negative curvature, as expected.

The parameters and carriers effective masses are given in the Tab. I.1.1.

The Luttinger hamiltonian is usually written in matrix form. In the $(u_{\Gamma_8,+\frac{3}{2}}, u_{\Gamma_8,-\frac{1}{2}}, u_{\Gamma_8,+\frac{1}{2}}, u_{\Gamma_8,-\frac{3}{2}})$ basis, we can rewrite it:

$$\mathcal{H}_L = -\frac{\hbar^2}{2m_0} \begin{pmatrix} a_{hh} & c & b & 0 \\ c^* & a_{lh} & 0 & -b \\ b^* & 0 & a_{lh} & c \\ 0 & -b^* & c^* & a_{hh} \end{pmatrix} \tag{I.8}$$

4

	CdTe	ZnTe
E_g	1606 meV	2391 meV
ε_r	10.6	9.7
a_0	6.48 Å	6.10 Å
Δ_{SO}	0.90 eV	0.91 eV
γ_1	4.8	4.07
γ_2	1.5	0.78
γ_3	1.9	1.59
$m_{hh,z}$	0.556	0.398
$m_{hh,\perp}$	0.159	0.206
$m_{lh,z}$	0.128	0.178
$m_{lh,\perp}$	0.303	0.303
m_e	0.096	0.116

Table I.1: Physical parameters for CdTe and ZnTe.

with:

$$a_{hh} = (\gamma_1 - 2\gamma_2)k_z^2 + (\gamma_1 + \gamma_2)k_\parallel^2$$
$$a_{lh} = (\gamma_1 + 2\gamma_2)k_z^2 + (\gamma_1 - \gamma_2)k_\parallel^2$$
$$b = -2\sqrt{3}\gamma_3(k_x - ik_y)k_z$$
$$c = -\sqrt{3}(\gamma_2(k_x^2 - k_y^2) - 2i\gamma_3 k_x k_y)$$

I.1.2   Lattice mismatch and the Bir-Pikus Hamiltonian

ZnTe crystal has a lattice parameter of $a_{ZnTe} = 6.10$ Å, while CdTe one is of $a_{CdTe} = 6.48$ Å. This lattice mismatch results in stress in a CdTe layer grown on a ZnTe substrate:

$$\varepsilon_\parallel = \frac{a_{ZnTe} - a_{CdTe}}{a_{CdTe}} = -5.8\% \tag{I.9}$$

In order to represent this strain and see its effect on the band, especially the Γ_8 band, we need to define a hamiltonian representing them. Strain deform the structure, so let's begin the representation with an volume $V = (x\mathbf{u_x} + y\mathbf{u_y} + z\mathbf{u_z}$, with $(\mathbf{u_x}, \mathbf{u_y}, \mathbf{u_z})$ an orthonormal basis. This volume will transform into another

one $V' = (x\mathbf{u_x'} + y\mathbf{u_y'} + z\mathbf{u_z'})$, where:

$$\begin{aligned}
\mathbf{u_x'} &= (1 + \varepsilon_{xx}')\mathbf{u_x} + \varepsilon_{xy}'\mathbf{u_y} + \varepsilon_{xz}'\mathbf{u_z} \\
\mathbf{u_y'} &= \varepsilon_{yx}'\mathbf{u_x} + (1 + \varepsilon_{yy}')\mathbf{u_y} + \varepsilon_{yz}'\mathbf{u_z} \\
\mathbf{u_z'} &= \varepsilon_{zx}'\mathbf{u_x} + \varepsilon_{zy}'\mathbf{u_y} + (1 + \varepsilon_{zz}')\mathbf{u_z}
\end{aligned} \tag{I.10}$$

ε_{ij}' represents an expansion of the vector i in the direction j. They are small deformation of the lattice, so we choose $|\varepsilon_{ij}'| \ll 1$. Such transformations can be decomposed in a symmetric part and an antisymetric one. We note $\bar{\bar{\varepsilon}}$ the symmetric part, called the strain tensor, defined such as:

$$\varepsilon_{ii} = \varepsilon_{ii}' \tag{I.11}$$

$$\varepsilon_{ij} = \frac{1}{2}\left(\varepsilon_{ij}' + \varepsilon_{ji}'\right) \tag{I.12}$$

In the linear regime, the strain tensor $\bar{\bar{\varepsilon}}$ is proportional to the stress tensor $\bar{\bar{\sigma}}$, where σ_{ij} describe a force parallel to i applied on a surface perpendicular to j. Therefore, σ_{ii} will describe an elongation or compression stress, while σ_{ij} $(i \neq j)$ represents a shear stress. Since these tensor are symmetric, we can reduce the number of coefficient from nine to six: σ_{xx}, σ_{yy}, σ_{zz}, $\sigma_{xy} = \sigma_{yx}$, $\sigma_{xz} = \sigma_{zx}$ and $\sigma_{yz} = \sigma_{zy}$. Therefore, in the linear regime and for a cubic crystal, we can write the Hooke's law:

$$\begin{bmatrix} \sigma_{xx} \\ \sigma_{yy} \\ \sigma_{zz} \\ \sigma_{xy} \\ \sigma_{xz} \\ \sigma_{yz} \end{bmatrix} = \begin{bmatrix} C_{11} & C_{12} & C_{12} & 0 & 0 & 0 \\ C_{12} & C_{11} & C_{12} & 0 & 0 & 0 \\ C_{12} & C_{12} & C_{11} & 0 & 0 & 0 \\ 0 & 0 & 0 & 2C_{44} & 0 & 0 \\ 0 & 0 & 0 & 0 & 2C_{44} & 0 \\ 0 & 0 & 0 & 0 & 0 & 2C_{44} \end{bmatrix} \begin{bmatrix} \varepsilon_{xx} \\ \varepsilon_{yy} \\ \varepsilon_{zz} \\ \varepsilon_{xy} \\ \varepsilon_{xz} \\ \varepsilon_{yz} \end{bmatrix} \tag{I.13}$$

Since x, y and z are physically equivalent, as well as xy, xz and yz, only two diagonal coefficient are needed, C_{11} and C_{44}. These coefficient coupling strains in a direction to a force in the same direction are obviously positives.

When the considered cube is compressed in one direction (e.g. $\varepsilon_{zz} < 0$), it will expand in the other direction in order to minimize elastic energy (ε_{xx}, $\varepsilon_{yy} > 0$ in the example). If we don't allow strain in these other directions ($\varepsilon_{xx} = \varepsilon_{yy} = 0$), a stress in the x and y directions had to be applied to keep the cube from expanding in these directions (σ_{xx}, $\sigma_{yy} < 0$ in the example). We can therefore physically expect $C_{12} > 0$.

The strain hamiltonian can be constructed noticing that the strain tensor $\bar{\bar{\varepsilon}}$ induces a shift in the bands energy, and that any ε_{ij} has the same symmetry as $k_i k_j$. The hamiltonian should then be formally identical to the Luttinger hamiltonian.

In the Γ_8 subspace, we can then use the Luttinger Hamiltonian, written in Eq. I.4, replacing the $k_i k_j$ by ε_{ij}. We obtain the Bir-Pikus Hamiltonian by replacing the γ_j parameters by the Bir-Pikus parameters a_ν, b_ν and d_ν [4]:

$$\mathcal{H}_{BP} = a_\nu \varepsilon I_4 + b_\nu \sum_i \varepsilon_{ii} \left(J_i^2 - \frac{1}{3}J^2 \right) + \frac{d_\nu}{\sqrt{3}}(\varepsilon_{xy}(J_x J_y + J_y J_x) + c.p) \qquad \text{(I.14)}$$

with $\varepsilon = Tr(\bar{\bar{\varepsilon}}) = \varepsilon_{xx} + \varepsilon_{yy} + \varepsilon_{zz}$.

The a_ν term, called the hydrostatic term, shifts the Γ_8 energy. The b_ν term represents the shear strain. In case of non-equal ε_{ii}, its effect is to lift up the two Γ_8 sub-bands as did a $k \neq 0$ in the Luttinger hamiltonian. The d_ν term, the pure shear strain (i.e ε_{ij} with $i \neq j$), has the same effect on the Γ_8 band.

One can notice that the Bir-Pikus hamiltonian is completely independant from $\mathbf{k}$, meaning that the band hamiltonian of a strain semiconductor is simply the sum of the Luttinger hamiltonian $\mathcal{H}_L$ (Eq. I.4) and the Bir-Pikus hamiltonian $\mathcal{H}_{BP}$ (Eq. I.14).

Let see how this apply to a CdTe layer deposited on a ZnTe layer. We define z as the growth direction. As shown at the begin of this part, CdTe and ZnTe have a lattice mismatch of 5.8%. Since both crystallize in a cubic lattice, the strain is the same in the x and y direction. We can then write the strain in the xy plane:

$$\varepsilon_{xx} = \varepsilon_{yy} = \varepsilon_\parallel = \frac{a_{ZnTe} - a_{CdTe}}{a_{CdTe}} \qquad \text{(I.15)}$$

In the z direction, however, no stress apply: the crystal is free to expand in this direction in order to reduce the elastic energy. Therefore, we can write $\sigma_{zz} = 0$ and, according to Hooke's law in Eq. I.13:

$$\begin{aligned} \sigma_{zz} &= C_{12}\varepsilon_{xx} + C_{12}\varepsilon_{yy} + C_{11}\varepsilon_{zz} \\ &= 0 \end{aligned} \qquad \text{(I.16)}$$

Using equality I.15, we can then deduce:

$$\varepsilon_{zz} = -\frac{2C_{12}}{C_{11}}\varepsilon_\parallel = -\frac{2C_{12}}{C_{11}}\frac{a_{ZnTe} - a_{CdTe}}{a_{CdTe}} \qquad \text{(I.17)}$$

Since we grow CdTe over a ZnTe substrate, the CdTe lattice is compressed in the plane, i.e. $\varepsilon_\parallel < 0$. Since C_{11}, $C_{12} > 0$ and $\varepsilon_\parallel < 0$ for CdTe over ZnTe (see Eq. I.15), one can easily deduce that $\varepsilon_{zz} > 0$. In the hypothesis of no defect created by the lattice mismatch, all the other strain terms are equal to zero. We can then decompose this strain into two component: a hydrostatic part describing the volume variation without breaking the cubic symmetry, and a shear part

introducing an anisotropy, breaking this symmetry:

$$\overline{\overline{\varepsilon_{hyd}}} = \frac{1}{3}(\varepsilon_{xx} + \varepsilon_{yy} + \varepsilon_{zz})I_3 \tag{I.18}$$

$$\overline{\overline{\varepsilon_{sh}}} = \overline{\overline{\varepsilon}} - \overline{\overline{\varepsilon_{hyd}}} \tag{I.19}$$

One can notice that $Tr(\overline{\overline{\varepsilon_{hyd}}}) = Tr(\overline{\overline{\varepsilon}}) = \varepsilon$. Since in the case of a hydrostatic compression, such as what is the case with CdTe over ZnTe, $\varepsilon_{hyd} < 0$, we then have $\varepsilon < 0$ and, according to the Bir-Pikus hamiltonian (Eq. I.14), the gap of CdTe increase. For CdTe, Bir-Pikus parameter are $a_\nu = 0.91$ eV, $b_\nu = 0.99$ eV and $d_\nu = 2.76$ eV [5].

Seeing that $\varepsilon_{ij} = 0$ for $i \neq j$, we can rewrite the Bir-Pikus hamiltonian without the shear strain term. Moreover, since $J^2 = J_x^2 + J_y^2 + J_z^2$ and that $\varepsilon_{xx} = \varepsilon_{yy} = \varepsilon_\parallel$, we can simplify this hamiltonian to:

$$\mathcal{H}_{BP,biax} = a_\nu \varepsilon I_4 + \frac{b_\nu}{3}(\varepsilon_\parallel - \varepsilon_{zz})(J_x^2 + J_y^2 - 2J_z^2) \tag{I.20}$$

And, since we are in the valence band with $J = \frac{3}{2}$ and $J_x^2 + J_y^2 + J_z^2 = J(J+1)I_4$, we can simplify the Bir-Pikus hamiltonian to its final form in the case of biaxal strain:

$$\mathcal{H}_{BP,biax} = \left(a_\nu \varepsilon + \frac{5}{4}b_\nu(\varepsilon_\nu - \varepsilon_{zz})\right)I_4 - b_\nu(\varepsilon_\nu - \varepsilon_{zz})J_z^2 \tag{I.21}$$

Using Eq. I.15 and I.17, we can easily calculate $\varepsilon_\parallel - \varepsilon_z$. Since $J_z|n\rangle = n|n\rangle$, we find:

$$
\begin{aligned}
E_{\pm\frac{3}{2}} - E_{\pm\frac{1}{2}} &= -2b_\nu\left(1 + \frac{2C_{12}}{C_{11}}\right)\frac{a_{ZnTe} - a_{CdTe}}{a_{CdTe}} \\
&= 2b_\nu\left(1 + \frac{2C_{12}}{C_{11}}\right)\frac{a_{CdTe} - a_{ZnTe}}{a_{CdTe}}
\end{aligned}
\tag{I.22}
$$

We find that, in a fully strained CdTe layer over a ZnTe substrate, the hh band is 300 meV above the lh one. In first approximation, we can then neglect the lh contribution in these nanostructures.

I.1.3   3D confinement: the quantum dot

Embedding a semiconductor in another one of larger creates trap for carrier, confining them in one or multiple. CdTe conduction band (resp. valence band) is a lower (resp. higher) energy than ZnTe ones, creating such a trap. Using the procedure described in Chap. ??, we can create nanometre size island of CdTe in a ZnTe lattice, effectively confining electron in all three directions, acting like a

3D trap for the free carriers. This lead to a quantization of the carriers energy levels and a discretization of the optical properties. This confinement being analogue to the Coulomb interaction of an isolated atom, such a structure is often dubbed "artificial atom". However, the interaction between the hole and the electron cannot be overlook, adding Coulomb interaction between the particule and the quasi-particle. It consists of an attractive term, shifting energy levels, and an exchange interaction (discussed in Sec. I.2.3). Moreover, the hole being the absence of an electron, its energy, charge, spin, orbital momentum, $\mathbf{k}$ and mass are, by definition, opposite to the missing electron. The electron-hole system has a hydrogen-like behaviour and is called an exciton.
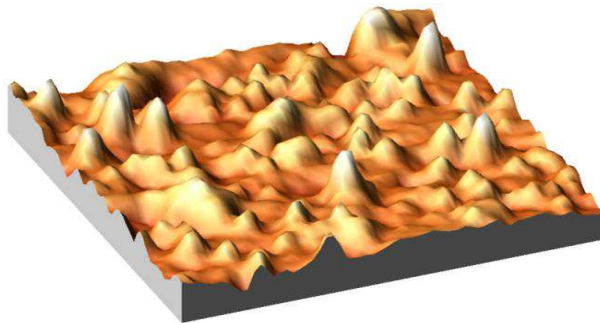

Figure I.3: Dots STM images

Before going to the exchange part, we will see the optical properties of this system. In order to do so, we develop the carrier wave-function on all the Bloch states:

$$\Psi(\mathbf{r}) = \sum_{n,\mathbf{k}} c_{n,\mathbf{k}} \psi_{n,\mathbf{k}} = \sum_{n,\mathbf{k}} c_{n,\mathbf{k}} u_{n,\mathbf{k}}(\mathbf{r}) \exp(i\mathbf{k}.\mathbf{r}) \tag{I.23}$$

Since we are in a confined environment, we can only consider the states around $\mathbf{k} = 0$. Since we consider the band extrema, we neglect the inter-band wave function mixing in a first time and use the effective-mass approximation. We can then limit the expansion of Bloch state to an expansion on the $u_{n,0}(\mathbf{r}) \exp(i\mathbf{k}.\mathbf{r})$, with $n = \Gamma_6$ for the conduction band and $n = \Gamma_8$ for the valence. We can then write:

$$\Psi_c(\mathbf{r}) \simeq \sum_{\mathbf{k}} c_{\mathbf{k}} u_{\Gamma_6,0}(\mathbf{r}) \exp(i\mathbf{k}.\mathbf{r}) = F_e(\mathbf{r}) u_{\Gamma_6,0} \tag{I.24}$$

$$\Psi_v(\mathbf{r}) \simeq \sum_{J_z=\{\pm\frac{3}{2},\pm\frac{1}{2}\},k} c_{J_z,\mathbf{k}} u_{\Gamma_8,J_z}(\mathbf{r}) \exp(i\mathbf{k}.\mathbf{r}) = \sum_{J_z=\{\pm\frac{3}{2},\pm\frac{1}{2}\}} F_{J_z}(\mathbf{r}) u_{\Gamma_8,J_z} \tag{I.25}$$

9

with $F_e(\mathbf{r}) = \sum_{\mathbf{k}} c_{\mathbf{k}} \exp(i\mathbf{k}.\mathbf{r})$ the electron envelop function and $F_{J_z}(\mathbf{r}) = c_{J_z,\mathbf{k}} \exp(i\mathbf{k}.\mathbf{r})$, $J_z = \{\pm\frac{3}{2}, \pm\frac{1}{2}\}$ the hole envelop functions.

The effective mass approximation allows us to replace the periodic crystal potential and the free-electron kinetic energy by the effective Hamiltonian representing the band extrema, using m_e for the conduction band and $\mathcal{H}_L + \mathcal{H}_{BP}$ for the top of the valence band. Considering the effective mass is the same in CdTe and ZnTe, we can now work with the simple picture of an effective mass carrier with the envelop function defined in Eqs. I.24 and I.25, trapped in a potential $V_e(\mathbf{r})$ for the conduction band or $V_h(\mathbf{r})$ for the valence band, creating by the band offset between the two semiconductors. We write the Schrödinger equations for these particle:

$$\left(\frac{\hbar^2}{2m_e}\Delta\right) F_e(\mathbf{r}) + V_e(\mathbf{r})F_e(\mathbf{r}) = E_e F_e(\mathbf{r}) \tag{I.26}$$

$$(\tilde{\mathcal{H}}_L + \tilde{\mathcal{H}}_{BP} + V_h(\mathbf{r})) \begin{pmatrix} F_{+\frac{3}{2}}(\mathbf{r}) \\ F_{+\frac{1}{2}}(\mathbf{r}) \\ F_{-\frac{1}{2}}(\mathbf{r}) \\ F_{-\frac{3}{2}}(\mathbf{r}) \end{pmatrix} = E_h \begin{pmatrix} F_{+\frac{3}{2}}(\mathbf{r}) \\ F_{+\frac{1}{2}}(\mathbf{r}) \\ F_{-\frac{1}{2}}(\mathbf{r}) \\ F_{-\frac{3}{2}}(\mathbf{r}) \end{pmatrix} \tag{I.27}$$

with $\tilde{\mathcal{H}}_L$ and $\tilde{\mathcal{H}}_{BP}$ the hole hamiltonians, opposite to the electron hamiltonians defined in Eq. I.4 and I.14. In $\tilde{\mathcal{H}}_L$, the k-terms transform into a gradient of the envelop function with the form $i\nabla$. For simplicity, the $\tilde{\ }$ will be dropped in the next equations. The derivation of the effective mass approximation can be found in reference [6].

In order to analytically solve these hamiltonian, another approximation is necessary. As discussed in section I.2, $\mathcal{H}_L$ couple the hh and lh through its non-diagonal terms, while $\mathcal{H}_{BP}$ lift their degeneracy, as shown in Sec. I.1.2. Considering the presence of biaxial strain, we can neglect the non-diagonal terms of $\mathcal{H}_L$ in regard to the action of $\mathcal{H}_{BP}$. This is the heavy hole approximation, uncoupling the four differential equations defined in Eq. I.27. Only the ground states $|\pm\frac{3}{2}\rangle$ are considered, with the effective mass given by the diagonal term of $\mathcal{H}_L$, noted $m_{h,\parallel}$ in the plane and $m_{h,z}$ along the growth axis.

In the general case, we still cannot solve this problem. However, it is possible for some chosen potential. Let's consider a lens like quantum dot, with a radius in the xy plane, noted ρ, much larger than it height L_z. We can therefore define two different harmonic oscillator of potential: a 2D oscillator $V_{c,v}(\rho)$ in the plane,

and a 1D oscillator $V_{c,v}(z)$ along the growth axis:

$$V_{c,v}(\rho) = 4\Delta E_{c,v} \frac{\rho^2}{L_z^2} \tag{I.28}$$

$$V_{c,v}(z) = 4\Delta E_{c,v} \frac{z^2}{L_z^2} \tag{I.29}$$

with $\Delta E_{c,v}$ the difference of conduction (resp. valence) band energy between the two semiconductors. The potential of the whole quantum dot will the be $V_{c,v}(\mathbf{r}) = V_{c,v}(\rho) + V_{c,v}(z)$. Separating the potential in those two parts means we are searching for solution of the form $F(z, \rho, \theta) = \chi(z)\phi_{n,m}(\rho, \theta)$, with θ the angle between the position vector and the x axis.

We write the characteristic spatial width and characteristic frequency of the 2D harmonic oscillator felt by the hole:

$$\Sigma_\rho^h = \sqrt{\frac{\hbar}{m_{h,\parallel}\omega_\rho^h}} \tag{I.30}$$

$$\omega_\rho^h = \sqrt{\frac{8\Delta E_v}{m_{h,\parallel}L_\rho^2}} \tag{I.31}$$

We can write the same equality along z replacing ρ by z and $m_{h,\parallel}$ by $m_{h,z}$. The same can be done for electron, replacing the $m_{h,\parallel}$ or $m_{h,z}$ by m_e and E_v by E_c.

We can find in textbook such as ref. [7] the solution of a harmonic oscillator from which we can deduce the solution for the ground state (GS) and the first two degenerated excited states. The first excited state is found to have an angular momentum $l_z = \pm 1$, and is then noted $Exc, \pm 1$. The envelop functions and energy are then found to be:

$$F_{c,v}^{GS}(z, \rho, \theta) = \frac{1}{\left(\sqrt{\pi}\Sigma_z\right)^{\frac{1}{2}}} \exp\left(-\frac{z^2}{2\Sigma_z^2}\right) \frac{1}{\left(\sqrt{\pi}\Sigma_\rho\right)^{\frac{1}{2}}} \exp\left(-\frac{\rho^2}{2\Sigma_\rho^2}\right) \tag{I.32}$$

$$E_{e,h}^{GS} = \hbar \frac{\omega_z^{e,h} + \omega_\rho^{e,h}}{2} \tag{I.33}$$

$$F_{c,v}^{Exc,\pm 1}(z, \rho, \theta) = \frac{1}{\left(\sqrt{\pi}\Sigma_z\right)^{\frac{1}{2}}} \exp\left(-\frac{z^2}{2\Sigma_z^2}\right) \frac{1}{\left(\sqrt{\pi}\Sigma_\rho\right)^{\frac{1}{2}}} \exp\left(-\frac{\rho^2}{2\Sigma_\rho^2}\right) \frac{\rho}{\sigma_\rho} \exp(\pm i\theta) \tag{I.34}$$

$$E_{e,h}^{Exc,\pm 1} = \hbar \frac{\omega_z^{e,h} + 3\omega_\rho^{e,h}}{2} \tag{I.35}$$

We see that this energy level are quantified in a way looking like an isolated atom, as pointed earlier. In reference to the atomic notation, the ground state, lower

energy level, is noted S and the two first degenerated level are noted P, even though atomic p-states usually are 3 fold degenerated.

One remarkable feature of the envelop functions is that both GS and the two first excited states present the same envelop along the z axis. The cause is directly the symmetry of the QD: since $L_z \ll L_\rho$, $\omega_z^{e,h} \gg \omega_\rho^{e,h}$, and since $E_{osc.\ harmo.} = (n + \frac{1}{2})\hbar\omega$, the next possible envelop function along the z axis is at higher energy than the next one in the plane. This geometry is also responsible for the 2 fold degeneracy of the P-states.

Both the GS and the excited states are once again degenerated due to the spin of the electron and the hole. The electron is in the conduction band with the Γ_6 symmetry: it can then take the value $\sigma_z = \pm\frac{1}{2}$ (noted $|\uparrow\rangle$ for $+\frac{1}{2}$ and $|\downarrow\rangle$ for $-\frac{1}{2}$). Since we are in the hh approximation, considering the lh are high enough energy to be negligible, the hole spin can only take the values $J_z = \pm\frac{3}{2}$ (noted $|\Uparrow\rangle$ for $+\frac{3}{2}$ and $|\Downarrow\rangle$ for $-\frac{3}{2}$). As pointed ahead, the hole is defined with the opposed characteristic of the missing electron (which may not be the one trapped in the QD). For instance, a hole $|\Downarrow\rangle$ corresponds to the absence of a valence electron $\Psi_v(\mathbf{r}) = u_{\Gamma_8,\frac{3}{2}}(\mathbf{r})F_{\frac{3}{2}}(\mathbf{r})$.

In order to find the optical properties of the quantum dot, we use the dipole approximation, giving the coupling to light as $H = -\frac{q}{m}\mathbf{p}.\mathbf{A}$, with $\mathbf{p}$ the momentum and $\mathbf{A}$ the vector potential. We can then determine the optical properties looking at the coupling through the $\mathbf{p}$ operator. In a QD, the light-matter interaction occur mainly through two processes: the absorption of a photon creating an exciton, and the recombination of an exciton emitting a photon. To model this, we consider the interband matrix element between the two electronic states Ψ_c and Ψ_v, as written in Eqs. I.24 and I.25:

$$|\langle\Psi_v|\mathbf{p}|\Psi_c\rangle|^2 = |\langle F_v|F_c\rangle|^2|\langle u_{\Gamma_8,J_z}|\mathbf{p}|u_{\Gamma_6,\sigma_z}\rangle|^2 \tag{I.36}$$

The first term is just the overlap of the envelop function, making sure the hole and the electron are of the right state: a transition between a P state of the valence band and a S state in the conduction band is then forbidden.

The second term, showing the interband matrix elements, depending only on the symmetry of the Bloch functions, will then draw the rule for the recombination. We write the spin states $|+\rangle$ and $|-\rangle$. Since, as shown in Sec. I.2, the conduction band is formed by s atomic states, we can now note them:

$$|u_{\Gamma_6,\uparrow}\rangle = |+\rangle \tag{I.37}$$
$$|u_{\Gamma_6,\downarrow}\rangle = |-\rangle \tag{I.38}$$

The valence, being formed by p atomic states, has to also take the $|X\rangle$, $|Y\rangle$ and $|Z\rangle$ electronic states. We can then write the three eigenstates of the electronic

part:

$$| + 1\rangle = -\frac{|X\rangle + i|Y\rangle}{\sqrt{2}} \tag{I.39}$$

$$|0\rangle = |Z\rangle \tag{I.40}$$

$$| - 1\rangle = \frac{|X\rangle - i|Y\rangle}{\sqrt{2}} \tag{I.41}$$

We can now write the states of the conduction band by composing these electronic states to the spin states:

$$|u_{\Gamma_8,+\frac{3}{2}}\rangle = | + 1\rangle|+\rangle \tag{I.42}$$

$$|u_{\Gamma_8,+\frac{1}{2}}\rangle = \sqrt{\frac{2}{3}}|0\rangle|+\rangle + \sqrt{\frac{2}{3}}| + 1\rangle|-\rangle \tag{I.43}$$

$$|u_{\Gamma_8,-\frac{1}{2}}\rangle = \sqrt{\frac{2}{3}}|0\rangle|-\rangle + \sqrt{\frac{2}{3}}| - 1\rangle|+\rangle \tag{I.44}$$

$$|u_{\Gamma_8,-\frac{3}{2}}\rangle = | - 1\rangle|-\rangle \tag{I.45}$$

Since we are working in the hh approximation, we neglect the contribution of the states $|u_{\Gamma_8,\pm\frac{1}{2}}\rangle$, calculating the interband matrix element only for $|u_{\Gamma_8,\pm\frac{3}{2}}\rangle$. Since $|+\rangle$ and $|-\rangle$ are orthogonal states, it is then clear that there is only two optically active transitions:

- between $|u_{\Gamma_6,\uparrow}\rangle$ and $|u_{\Gamma_8,+\frac{3}{2}}\rangle$ (hole $| \Downarrow\rangle$), coupled by $p_- = p_x - ip_y$, corresponding to σ_- photon absorption or emission.

- between $|u_{\Gamma_6,\downarrow}\rangle$ and $|u_{\Gamma_8,-\frac{3}{2}}\rangle$ (hole $| \Uparrow\rangle$), coupled by $p_+ = p_x + ip_y$, corresponding to σ_+ photon absorption or emission.

We see thus that, for an exciton in the S state of the QD, four configurations are possible. First, we have the bright states $| \uparrow\Downarrow\rangle$, with an angular momentum $X_z = \sigma_z + J_z = \frac{1}{2} - \frac{3}{2} = -1$, and $| \downarrow\Uparrow\rangle$, with an angular momentum $X_z = -\frac{1}{2} + \frac{3}{2} = +1$. Both of these states are optically active, meaning their transitions are permitted and they can recombine radiatively. Two other states can exists, called dark states: $| \uparrow\Uparrow\rangle$, with an angular momentum $X_z = +2$, and $| \downarrow\Downarrow\rangle$, with an angular momentum $X_z = -2$.

Approximating the QD potential as harmonic usually overestimate the confinement, and thus the single-particle energy. But the wave-functions found in this chapter can still be used as trial wave-functions for variational calculations in other potential, in order to estimate the correct energy level.

We discussed in this chapter about the neutral exciton (X), formed by a single electron-hole pair. However, several types of exciton can be observed in a quantum

dots. First to consider are the charged excitons. In this case, a supplementary charge is injected in the QD in addition to the exciton, forming a hole-hole-electron (X^+) or hole-electron-electron (X^-) complex. It also happen that two exciton with opposed spins are trapped in a dot. This complex is called biexciton, noted X^2, and relax to leave a single neutral exciton in the QD. Charged biexciton and other multi-exciton complex also exist but are not discussed on the thesis. Even if the physics of each of this system is different, the selection rule devised in this chapter apply to all of them.
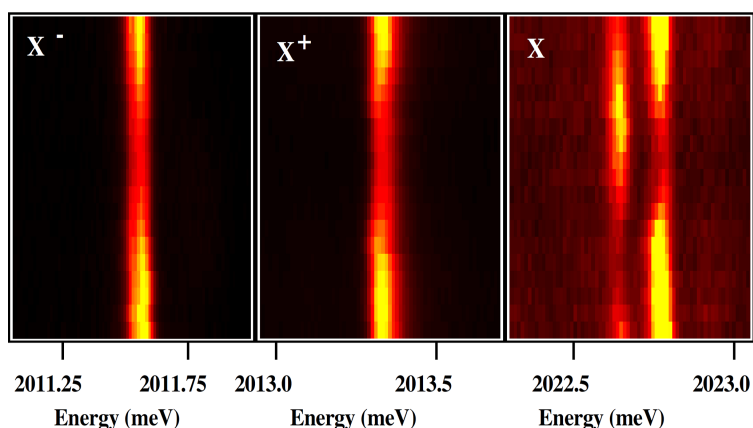
I.1.4   Valence band mixing

Figure I.4: Linear polarization of empty dot

This simple picture, however, don't represent accurately most of the experiment. In a lot of found dots, both X and X^2 present two peaks with linear polarization dependency, as presented in Fig. I.4. This picture could be explained by the long-range exchange interaction, presented in Sec. I.2.1. However, it predicts an angle between the two linearly polarized states of 90°, while the observed angle is far from this value. Moreover, in charged species, the electron (resp. hole) interact with two holes (resp. electrons) with opposite spins, leading to an absence of exchange interaction. Therefore, in the hh approximation, neither X^+ nor X^- should present linear polarization dependency. However, such a dependency can be observed in actual dots.

However, we saw in Sec. I.1.3 that the hh approximation supposed neglecting lh contribution in the Luttinger hamiltonian, through the presence of biaxial strain lifting their degeneracy with hh. However, we can see in the Bir-Pikus hamiltonian (Eq. I.14) that introducing an anisotropic distribution of strain ($\varepsilon_{xx} \neq \varepsilon_{yy}$ or

14

$\varepsilon_{ij} \neq 0$ with $i \neq j$) can mix hh states $J_z = \pm\frac{3}{2}$ and lh states $J_z = \mp\frac{1}{2}$. Such a mixing, called Valence Band Mixing (VBM) can also occur through the Luttinger hamltonian in an anisotropic dot ($L_x \neq L_y$), but it would be weaker than the one occurring through Bir-Pikus hamiltonian.

Looking at the matrix form of the Luttinger hamiltonian in Eq. I.8, we see that $\pm\frac{3}{2}$ could also be coupled to $\pm\frac{1}{2}$ through the b term. However, we supposed that the wave function can be separated into a pure z component and a pure $x - y$ one, meaning $\langle \chi_i(z)|k_z|\chi_j(z)\rangle = 0$ with $\chi_{(i,j)}(z)$ define in Eqs. I.32 and I.34. This means b doesn't couple envelop functions. A similar coupling parameter appear in the Bir-Pikus hamiltonian due to the shear strains ε_{zx} and ε_{zy}. However, in most of the found dots, ε_{zx} and ε_{zy} is found to be negligible [8].

The envelop function mainly test the overlap and the energy state of the exciton. It doesn't affect light polarization. Therefore, in order to understand the effects of the VBM on the polarization of the dot emission, we can neglect them, only looking at the spin component. We also neglect the envelop function difference between hh and lh. We can then describe the coupling by redefining up and down hole spins as a superposition of $\pm\frac{3}{2}$ and $\mp\frac{1}{2}$. This lh part will be written through a phenomenological parameter $\eta \exp(2i\theta)$ with θ the direction of the strain:

$$|\tilde{\Uparrow}\rangle \propto | + \frac{3}{2}\rangle - \eta \exp(2i\theta)| - \frac{1}{2}\rangle \tag{I.46}$$

$$|\tilde{\Downarrow}\rangle \propto | - \frac{3}{2}\rangle - \eta \exp(2i\theta)| + \frac{1}{2}\rangle \tag{I.47}$$

with, in the hypothesis of a small strain-induced VBM:

$$\eta \exp(2i\theta) = \frac{1}{\Delta_{lh}}(id\varepsilon_{xy} - b(\varepsilon_{xx} - \varepsilon_{yy})) \tag{I.48}$$

with Δ_{lh} the lh-hh splitting given by the average in-plane bi-axial strain $b(\varepsilon_{xx} = \varepsilon_{yy} + 2\varepsilon_{zz})$. However, experimentally, we can only access $\eta = \frac{E}{\Delta_{lh}}$, with E the anisotropy of strain.

To see the effect of the VBM on the polarization, we begin to consider the emission of an charged state, where the exchange interaction doesn't affect it. We write the polarization of the detection $\mathbf{e} = \cos(\alpha)\mathbf{e_x} + \sin(\alpha)\mathbf{e_y}$. We then can find the oscillator strength of the transition:

$$\begin{aligned} \Omega(\alpha) &\propto |\langle \uparrow | \cos(\alpha)p_X + \sin(\alpha)o_Y | \uparrow\downarrow \tilde{\Uparrow}\rangle|^2 \\ &= 1 + \frac{\eta^2}{3} + \frac{2}{\sqrt{3}}\eta \cos(2(\theta - \alpha)) \end{aligned} \tag{I.49}$$

There is then a dependency in linear polarization of the emission, depending on the angle between the polariser and the direction on the strain. In the experiment, no

correlation where observed between the polarisation axis of the different quantum dots [9], as can be expected from the random strain relaxation forming the dots as presented in Chap. ??.

We saw that the presence of an anisotropy of strain lead to Valence Band Mixing, characterized a linear polarization dependency of the charged exciton emission. A similar effect is observed on neutral exciton. However, in order to understand the emission of this complex, the exchange also has to be taken into account. It will be discussed and conclude in Sec. I.2.3. It should be noted that dark state are also coupled to each other by η, acquiring a weak oscillator with a dipole along z. More complete has been done by Yoan Léger in Ref. [8] and [9], taking into account the effective mass carriers envelop functions, and doing calculation beyond the limit of small VBM.

I.2 Exchange interaction between carrier and magnetic atom

I.2.1 Exchange interaction in Diluted Magnetic Semiconductors

We were interested until now at the structure of a so-called perfect semiconductor, without defect or impurity. However, we are interested in thesis to introduce a low density of either Manganese or Chromium atom in the crystal, namely, an impurity. A semiconductor doped in this fashion is called Diluted Magnetic Semiconductor (DMS). This magnetic atom will interact with the semiconductor electrons via its localized electron on its exterior shell. For Mn and Cr, this orbital is the d orbital, so it will be the one considered in the following document. From the interaction between these electron and the one in the conduction band of the semi-conductor, new properties will arise. We can easily write this interaction as a "Heisenberg" interaction. With $|S\rangle$ as the electronic spin of the magnetic impurity and, as previously, $|\sigma\rangle$ as the spin of the conduction electron, we can write:

$$\mathcal{H}_{Heisenberg} = I\boldsymbol{\sigma}.\mathbf{S} \tag{I.50}$$

with I the interaction constant. We write $\boldsymbol{\sigma}$ and $\mathbf{S}$ in the form of Pauli matrix. Namely, for a spin $\frac{1}{2}$ such as $\boldsymbol{\sigma}$, these writes as:

$$
\begin{aligned}
\sigma_x &= \frac{\hbar}{2}\begin{pmatrix} 0 & 1 \\ 1 & 0 \end{pmatrix} \\
\sigma_y &= \frac{\hbar}{2}\begin{pmatrix} 0 & -i \\ i & 0 \end{pmatrix} \\
\sigma_z &= \frac{\hbar}{2}\begin{pmatrix} 1 & 0 \\ 0 & -1 \end{pmatrix}
\end{aligned}
\tag{I.51}
$$

This formally simple interaction represents the Pauli exclusion principle through the interaction between two spins. Almost all the interaction in this chapter will be of this form, although presenting different physical process, with only the interaction constant I varying from one another.

The inserted impurities didn't modify the crystal structure, meaning the semiconductor wave function will not be significantly altered by them. We can then as usual note the conduction electron wave function as $|\psi_{\mathbf{k}}\rangle|\sigma;\sigma_z\rangle \equiv |\psi_{\mathbf{k}};\sigma_z\rangle$, $|\psi_{\mathbf{k}}\rangle$ being the Bloch function of the semiconductor. On the other side, considering a magnetic atom at $\mathbf{r} = \mathbf{R_d}$, we write the spatial component of the wave function $\Phi_d(\mathbf{r} - \mathbf{R_d})$. Its total electronic spin, sum of the electron spins on its d orbital, is noted $|S;S_z\rangle$. The whole wave function of the magnetic atom is then $|\Phi_d;S_Z\rangle$.

Using Born-Oppenheimer approximation, we can write the hamiltonian for these electrons:

$$
\mathcal{H}_{BO} = \sum_i \left(\frac{p_i^2}{2m_c} + V_c(\mathbf{r}_i) \right) + \frac{1}{2}\sum_{i,j} \frac{e^2}{4\pi\varepsilon_0|\mathbf{r_i} - \mathbf{r_j}|}
\tag{I.52}
$$

This first is a single particle hamiltonian, taking into account the kinetic energy of the electron and the crystal potential $V_c(\mathbf{r}_i)$ felt by the electron at the position $\mathbf{r}_i$. This potential include the impurities potential, meaning it will be different at the impurities positions than elsewhere in the semiconductor. The final term represents the Coulomb interaction between the electrons.

We can rewrite this hamiltonian using second quantification. We define the destruction (resp. creation) operator of a particle in the conduction band at the wave vector $\mathbf{k}$ and the spin σ as $a_{\mathbf{k},\sigma}$ (resp. $a_{\mathbf{k},\sigma}^\dagger$). In the same fashion, we define the destruction (resp. creation) operator of the electronic level of an impurity as $a_{d,S}$ (resp. $a_{d,S}^\dagger$). Supposing the number of electron on the d orbital of the magnetic

atoms doesn't change, the hamiltonian I.52 then become:

$$\mathcal{H}_{SQ} = \sum_{\mathbf{k},\sigma} E_{\mathbf{k}} a_{\mathbf{k},\sigma}^{\dagger} a_{\mathbf{k},\sigma} + \sum_{S} E_d a_{d,S}^{\dagger} a_{d,S} + \sum_{\mathbf{k},\mathbf{k}'} U_{\mathbf{k},\mathbf{k}'} a_{\mathbf{k},\sigma}^{\dagger} a_{\mathbf{k}',\sigma}$$

$$+ \sum_{\mathbf{k},\sigma,S} M_{\mathbf{k}} (a_{\mathbf{k},\sigma}^{\dagger} a_{d,S} + a_{d,S}^{\dagger} a_{\mathbf{k},\sigma}) + \frac{1}{2} \sum_{i,j,k,l} V_{i,j,m,n} a_i^{\dagger} a_j^{\dagger} a_n a_m \quad \text{(I.53)}$$

$$= \mathcal{H}_0 + \mathcal{H}_d + V_d + \mathcal{H}_{hyb} + \mathcal{H}_{Coulomb}$$

The constant electron number supposition is good enough for the picture we want to draw since most of the spin-driven interaction do not induce a change of this number.

$\mathcal{H}_0$ represents the energy of the unperturbed wave function of the semiconductor, with E_k the energy of an electron with the wave vector $\mathbf{k}$.

$\mathcal{H}_d$ is the same as $\mathcal{H}_0$ but for an electron of the d orbital of the considered magnetic impurity, with E_d the energy of an electron on this orbital.

V_d represents the impurities potential, allowing the semiconductor electrons to scatter on it. However, Mn and Cr does not modify strongly the crystal potential. We can then consider that the states of the semiconductor $|\psi_k\rangle$ are also solution of the full crystal potential, including impurity, and neglect this term.

$\mathcal{H}_{hyb}$ mix the semiconductor states with the states of the impurities. It represents an exchange interaction between an electron of the semiconductor and one of the d orbital of an impurity. It is also called the Anderson hamiltonian. We can write the exchange constant as:

$$V_{kd} = \int \mathrm{d}\mathbf{r} \psi_k^*(\mathbf{r}) \mathcal{H}_1 \Phi_d(\mathbf{r} - \mathbf{R_d}) \quad \text{(I.54)}$$

with $\mathcal{H}_1$ the one particle hamiltonian. This term depend on the Bloch state of both the semiconductor and the impurity, meaning it can be reduce to zero by the symmetry of such functions in some specific cases.

Let's now focus on last term, $\mathcal{H}_{Coulomb}$, representing the two particles exchange $\mathcal{H}_{Coulomb}$. i, j, m and n each represents a full wave function, both spatial and spin part, and can be either a electron of the semiconductor or of one of the impurities. We can then separate this hamiltonian in three different term depending on the value of i, j, m and n and illustrated in Fig. I.5.

We first consider two states belonging to the continuum, appearing as J_1 on the diagram. As shown in [10], we can treat the interaction between one electron in the conduction band and the $N - 1$ electrons of the valence band as an interaction between this electron and the corresponding hole, with an adding exchange interaction. We can then write the exchange hamiltonian in a Heisenberg form as:

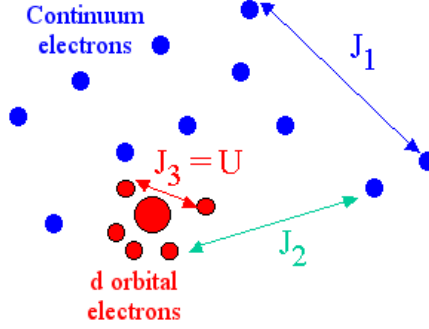$$\mathcal{H}_{eh} = I_{eh} \boldsymbol{\sigma}.\mathbf{J} \quad \text{(I.55)}$$

Figure I.5: Carrier interaction with no change of the number of electron on the impurity, derived from the hamiltonian $\mathcal{H}_{Coulomb}$.

The matrix elements being:

$$\langle e, h|\mathcal{H}_{SC}^{exch}|e', h'\rangle = \delta_{h,h'}\delta_{e,e'}(\epsilon_e - \epsilon_h) - K_{h'ee'h} + I_{eh'e'h} \qquad (I.56)$$

with $\epsilon_{e,h}$ the energy level of the electron and hole, $K_{h'ee'h}$ the direct Coulomb interaction and $I_{eh'e'h}$ the exchange Coulomb interaction. As classically expected from an electric interaction between two opposite charges, the direct Coulomb interaction is attractive and therefore lower the overall energy of the system.

$I_{eh'e'h}$ is written:

$$I_{eh'e'h} = \frac{e^2}{4\pi\varepsilon} \int \mathrm{d}\mathbf{r}_1\mathrm{d}\mathbf{r}_2 \frac{\psi_c^*(\mathbf{r}_1)\psi_{v'}^*(\mathbf{r}_2)\psi_{c'}(\mathbf{r}_2)\psi_v(\mathbf{r}_1)}{|\mathbf{r}_1 - \mathbf{r}_2|} \qquad (I.57)$$

with ε the dielectric constant and ψ_v the wave function of the missing exciton. One can see that it is different from zero only if the spin of the electron and the hole are opposite (meaning the spin of both electrons are the same). Since its value is positive for opposite electron and hole spins, this term will increase the energy of the bright states while the dark one remain unaffected. It results in a ferromagnetic effective hamiltonian lifting the degeneracy between between bright and dark states.

Taking into account the symmetry of the crystal, Bir and Pikus demonstrated that the complete hamiltonian can be decomposed in two different components: For an electron and a hole in the same Brillouin zone, the short-range exchange interaction is to be considered. It can be written:

$$I_{eh}^{sr} = \delta_0^{sr}\boldsymbol{\sigma}.\mathbf{J} + \delta_2 \sum_{i=x,y,z} \sigma_i J_i^3 \qquad (I.58)$$

The first term lift the degeneracy between exciton of total angular moment $X = 2$ and $X = 1$. The second one was found through symmetry considerations and gives

the dark states a fine structure. This have never been observed experimentally in bulk semiconductor, but it is expected to be much smaller than the lift induced by δ_0.

For carriers in different Brillouin-zone, the long-range exchange interaction have to be considered. It lifts up the degeneracy between transverse exciton, with a dipole perpendicular to the center of mass $\mathbf{k}_e x$, and longitudinal exciton, with a dipole parallel to $\mathbf{k}_e x$. This splitting is independent of $\mathbf{k}_e x$ value for $\mathbf{k}_e x > \dfrac{2\pi}{\lambda}$. The case $\mathbf{k}_e x < \dfrac{2\pi}{\lambda}$ leads to light-matter strong-coupling regime and is beyond the scope of the thesis.

The next interaction we consider is the one of two electrons from a localized atom. It represents internal transitions of the atom, representing the Hund rule. It is written:

$$\mathcal{H}_U = \sum_{d,S,S'} U a_{d,S}^\dagger a_{d,S'}^\dagger a_{d,S'} a_{d,S'} \tag{I.59}$$

with $U = \int \mathrm{d}\mathbf{r}\mathrm{d}\mathbf{r}' \dfrac{e^2}{4\pi\varepsilon_0|\mathbf{r}-\mathbf{r}'|}|\Phi_d(\mathbf{r})|^2|\Phi_d(\mathbf{r}')|^2$ the Coulomb interaction between two electrons on the same orbital with different spins. Thus, it costs more energy to add an electron on the same orbital than on another. We find back the Hund rule, with electron first filing all orbitals with parallel spin before adding an electron to an orbital with another one, with opposed spin.

The third considered interaction is the one between an electron from the magnetic atom and an electron from the semiconductor. In the same fashion as with carriers of the bulk, it can be separated in two terms that will be developed in the next paragraphs: a direct Coulomb interaction between the two electrons, and an exchange interaction arising from the fermionic nature of electrons.

The direct Coulomb interaction doesn't depends on electrons spins. It only act on the total energy of the system and is therefore only needed when searching the total energy of an exciton. We write it:

$$K = + \sum_{\mathbf{k},\sigma,\sigma'} K_\mathbf{k} a_{\mathbf{k},\sigma}^\dagger a_{d,\sigma'}^\dagger a_{d,\sigma'} a_{\mathbf{k},\sigma} \tag{I.60}$$

with

$$K_k = \int \mathrm{d}\mathbf{r}\mathrm{d}\mathbf{r}' |\psi_k(\mathbf{r})|^2 \dfrac{e^2}{4\pi\varepsilon_0|\mathbf{r}'-\mathbf{r}|}|\Phi_d(\mathbf{r}')|^2$$

It is clear that the spin σ (resp. σ') of the k electron (resp. d electron) is not changed by this interaction. Since it only induce a shift in the total energy, we can redefine the energy axis to ignore it.

To go to the second term, the exchange interaction, we write it in second quantification:

$$J = + \sum_{k,k',\sigma,\sigma'} I^{ex}_{kk'} a^\dagger_{k',\sigma} a^\dagger_{d,\sigma'} a_{k,\sigma'} a_{d,\sigma} = + \sum_{k,k',\sigma,\sigma'} J_{kk'} a^\dagger_{k',\sigma} a_{k,\sigma'} a^\dagger_{d,\sigma'} a_{d,\sigma} \qquad \text{(I.61)}$$

with

$$I^{ex}_{kk'} = \int d\mathbf{r} d\mathbf{r}' \psi^*_{k'}(\mathbf{r}) \psi^*_k(\mathbf{r}') \frac{e^2}{4\pi\varepsilon_0 |\mathbf{r}' - \mathbf{r}|} \Phi^*_d(\mathbf{r}) \Phi^*_d(\mathbf{r}') \qquad \text{(I.62)}$$

As can be sawn on Eq. I.61, this interaction exchange the spin σ and σ' of both electrons, thus its name. However, I.62 shows that the spin interaction comes from a Coulomb interaction between two fermions.

We define:

$$\begin{aligned} \sigma^z_{kk'} &= a^\dagger_{k,\sigma} a_{k',\sigma} - a^\dagger_{k,-\sigma} a_{k',-\sigma} \\ \sigma^+_{kk'} &= a^\dagger_{k,\sigma} a_{k',-\sigma} \\ \sigma^-_{kk'} &= a^\dagger_{k,-\sigma} a_{k',\sigma} \end{aligned} \qquad \text{(I.63)}$$

Considering now that this interaction does not change the number of electrons on the d orbital of the considered magnetic atom, we can find the Kondo hamiltonian:

$$\mathcal{H}_{sd} = - \sum_{k,k'} I^{ex}_{kk'} \boldsymbol{\sigma}_{k,k'} . \mathbf{S} \qquad \text{(I.64)}$$

Since $I^{ex}_{k,k'}$ is positive, the negative sign in front of the Kondo hamiltonian shows that the energy minimum is reached when the spins of both electron are aligned, and is therefore ferromagnetic.

We can now write the hamiltonian I.53, detailing these new hamiltonians:

$$\mathcal{H}_{SQ} = \mathcal{H}_0 + \mathcal{H}_d + \mathcal{H}_{hyb} + \mathcal{H}_{eh} + \mathcal{H}_U + \mathcal{H}_{sd} \qquad \text{(I.65)}$$

with the exchange constant in $\mathcal{H}_{hyb}$, $V_{kd} = \int d\mathbf{r} \psi^*_k(\mathbf{r}) \mathcal{H}_1 \Phi_d(\mathbf{r} - \mathbf{R_d})$.

We now have two hamiltonians to model the exchange interaction between the impurities electrons and the one in the conduction band of the semiconductor: $\mathcal{H}_{hyb}$ and $\mathcal{H}_{sd}$. Schrieffer and Wolff rewrote Anderson hamiltonian in order to give a form closer to the Kondo hamiltonian [11]:

$$\begin{aligned} \mathcal{H}_{hyb} &= \sum_{k,k'} V_{kd} V_{k'd} \left(\frac{1}{E_k - (E_d + U)} + \frac{1}{E_{k'} - (E_d + U)} \right. \\ &\qquad\qquad \left. - \frac{1}{E_k - E_d} - \frac{1}{E_{k'} - E_d} \right) a^\dagger_{k',\sigma} a_{k,-\sigma} a^\dagger_{d,S-2\sigma} a_{d,S} \\ &= \sum_{k,k'} I^{hyb}_{kk'} a^\dagger_{k',\sigma} a_{k,-\sigma} a^\dagger_{d,S-2\sigma} a_{d,S} \qquad \text{(I.66)} \end{aligned}$$

The Fig. I.6 illustrates the different energies introduced in I.66, presenting virtual transition to the d orbital of the magnetic atom. The two possible energies are E_d for the low energy level, and $E_d + U$ for the high energy one, U being the energy needed to add an electron to the orbital.
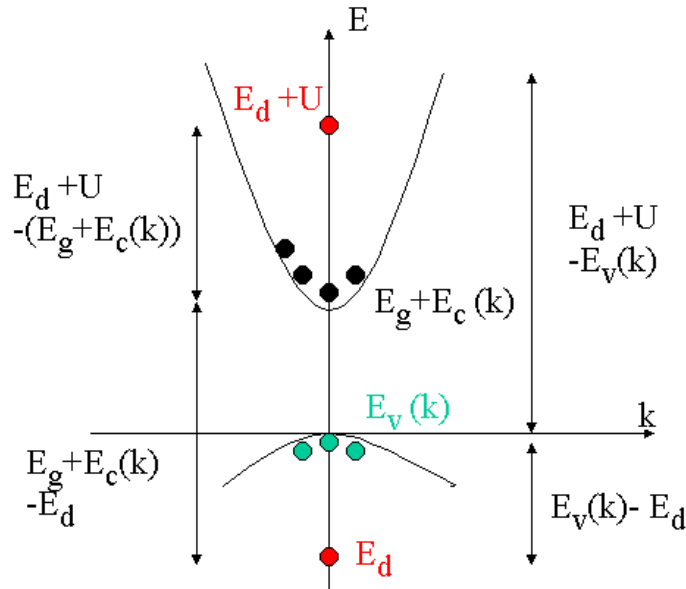

Figure I.6: Schema of the band structure and virtal transitions between valence band and conduction band.

Doing this transformation is an important step, since we are now able to use a Heisenberg type spin hamiltonian instead of a hamiltonian mixing wave function, in addition to having the same formalism to write both type of exchange interactions, with just a difference in the exchange constants $I_{kk'}^{ex}$ and $I_{kk'}^{hyb}$.

Supposing the coupling occur between two electrons with a close k $(k \simeq k')$, we can rewrite $I_{kk'}^{hyb}$ as:

$$
\begin{aligned}
I_{kk'}^{hyb} &= 2|V_{kd}|^2 \frac{U}{(E_k - E_d)(E_k - (E_d + U))} \\
&= -2|V_{kd}|^2 \frac{U}{(E_k - E_d)(E_d + U - E_k)}
\end{aligned}
\tag{I.67}
$$

Looking ath the Fig. I.6, one can see that U and $E_k - E_d$ are both positive, while $E_k - (E_d + U)$ is negative. Thus, $I_{kk'}^{hyb}$ is negative, and we see that, while exchange leads to a ferromagnetic coupling, hybridization leads to an anti-ferromagnetic one.

There will be a competition in the semiconductor between these two for every type of carrier.

Reusing the hypothesis done on Sec. I.2 of small k value, and the value of V_{kd} presented in Eq. I.54, we can rewrite the exchange constant:

$$I_{00,\{c,v\}}^{hyb} = -2 \left(\frac{U}{(E_{\{c,v\}}(0) - E_d)(E_d + U - E_{\{c,v\}}(0))} \right) \int \mathrm{d}\mathbf{r}\Phi_r^*(\mathbf{r})\mathcal{H}_1\psi_0^{\{c,v\}} \quad \text{(I.68)}$$

$$I_{00,\{c,v\}}^{ex} = \int \mathrm{d}\mathbf{r}\mathrm{d}\mathbf{r}'\psi_0^{*\{c,v\}}(\mathbf{r})\Psi_d^* \frac{e^2}{4\pi\varepsilon_0|\mathbf{r}' - \mathbf{r}|}\psi_0^{\{c,v\}}(\mathbf{r})\Psi_d(\mathbf{r}) \quad \text{(I.69)}$$

In the valence band, the semiconductor have the p symmetry, as discussed in Sec. I.2. We then write I_{pd} as the sum of the hybridization and the exchange contributions:

$$I_{pd} = I_{00,v}^{hyb} + I_{00,v}^{ex} \quad \text{(I.70)}$$

In the conduction band, the orbital are s, and so we will write the interaction I_{sd}. However, since s orbital have a spherical symmetry, there is no hybridization contribution. The expression is then pretty easy:

$$I_{sd} = I_{00,c}^{ex} \quad \text{(I.71)}$$

Having define those, we can now rewrite the Hamiltonian of the interaction with one magnetic atom in the Heisenberg notation:

$$\begin{aligned} \mathcal{H}_{SQ} &= \mathcal{H}_0 \; + \; \mathcal{H}_{eh} \; + \; \underbrace{I_{sd}\boldsymbol{\sigma}.\mathbf{S}}_{\mathcal{H}_{sd}} \; + \; \underbrace{I_{pd}\mathbf{J}.\mathbf{S}}_{\mathcal{H}_{pd}} \\ &= \mathcal{H}_0 \; + \; \mathcal{H}_{eh} \; + \; \mathcal{H}_{sd} \; + \; \mathcal{H}_{pd} \end{aligned} \quad \text{(I.72)}$$

Since a DMS contain a small percentage of magnetic atoms, we can write the hamiltonian of the full semiconductor by summing on their position. We finally get:

$$\mathcal{H}_{DMS} = \mathcal{H}_0 \qquad + \mathcal{H}_{eh} \qquad + \sum_i I_{sd}(\mathbf{R}_i)\boldsymbol{\sigma}.\mathbf{S}_i \qquad + \sum_i I_{pd}(\mathbf{R}_i)\mathbf{J}.\mathbf{S}_i \quad \text{(I.73)}$$

This can be further simplified with two approximations. First, since conduction electron sees a lot of different atomic sites, we can we can work with the mean value of the magnetic atoms spins, $\langle\mathbf{S}\rangle$, instead of their individual value $\mathbf{S}_i$. This is the mean field approximation, the magnetic atoms being seen as a magnetic field. And for the same reason, we can consider the interaction with each site of the crystal multiplied by the probability x of being occupied by a magnetic atom,

instead of summing only on the magnetic atoms positions. This is the virtual crystal approximation. We can then rewrite:

$$\sum_i I_{sd}(\mathbf{R}_i)\boldsymbol{\sigma}.\mathbf{S}_i = x\sum_{\mathbf{R}} I_{sd}(\mathbf{R})\boldsymbol{\sigma}.\langle\mathbf{S}\rangle \tag{I.74}$$

Projecting along the quantization axis, we just replace $\boldsymbol{\sigma}.\langle\mathbf{S}\rangle$ by $\sigma_z\langle S_z\rangle$. Since the atoms are seen as a magnetic field, they induce a degeneracy lift ΔE_c between the two spin values of conduction electron, $|\sigma_z = \pm\frac{1}{2}\rangle$:

$$\Delta E_c = N_0 x\alpha\sigma_z\langle S_z\rangle \tag{I.75}$$

with $\alpha \propto I_{sd}^{00}$ the interaction constant between impurity and conduction band Bloch function at $\mathbf{k} = 0$, and N_0 the number of cell per volume.

The same consideration can be done for valence band. Hh and lh are separated via their spin values: $|J_z = \pm\frac{3}{2}\rangle$ for hh, $|J_z = \pm\frac{1}{2}\rangle$ for lh. We then get:

$$\Delta E_v = N_0 x\frac{\beta}{3}J_z\langle S_z\rangle \tag{I.76}$$

with $\beta \propto I_{pd}^{00}$ the interaction constant between impurity and conduction band Bloch function at $\mathbf{k} = 0$.

To be completely thorough with the analysis, we should also take into account the confinement due to the quantum dot. This means the wave vector $\mathbf{k}$ of the carriers can be different from 0, leading to small perturbative effect on $\mathcal{H}_{sd}$ and $\mathcal{H}_{pd}$. This was done thoroughly by Laurent Maingault in the Chap. I.3 of his PhD thesis [12]. It is shown that the hamiltonian changed as follow:

$$\mathcal{H}_{sd}(\mathbf{R}) = -\alpha\boldsymbol{\sigma}.\mathbf{S}\left|F(\mathbf{R}) - A_2\left(\frac{\partial^2 F}{\partial z^2}(\mathbf{R}) + \frac{\partial^2 F}{\partial\rho^2}(\mathbf{R})\right)\right|^2$$
$$- \beta\boldsymbol{\sigma}.\mathbf{S}\left((C_2 - B_2)\left|\frac{\partial^2 F}{\partial z^2}(\mathbf{R})\right|^2 + C_2\left|\frac{\partial^2 F}{\partial\rho^2}(\mathbf{R})\right|^2\right) \tag{I.77}$$
$$\mathcal{H}_{pd}(\mathbf{R}) = -\beta\mathbf{J}.\mathbf{S}|F(\mathbf{R}) - V_{kd}F''(\mathbf{R})|^2 \tag{I.78}$$

with $F(\mathbf{R})$ the carrier envelop function defined in I.24 and I.25, $F''(\mathbf{R})$ the second derivative of this wave function, and A_2, B_2, C_2 constant depending on the semiconductor lattice. For CdTe, $A_2 = 10.3$ Å^{-2}, $B_2 = 0.781$ Å^{-2} and $C_2 = 19.8$ Å^{-2}.

I.2.2   Studied magnetic atoms: Mn and Cr

Mn in CdTe

For the Mn, we will rewrite the hamiltonian the exchange interaction in the valence band I_{pd} as I_{hMn} and I_{sd} in the conduction band as I_{eMn}, since we look at the interaction between an exciton and the Manganese atom. The hamiltonian I.72 is then rewrited:

$$\mathcal{H}_{Mn} = \mathcal{H}_0 + \mathcal{H}_{eMn} + \mathcal{H}_{hMn} \tag{I.79}$$

In the conduction band, the electrons s orbital are orthogonal to the d orbital of the Mn atom. No hybridization can then occur between these. Only the Coulomd interaction remain, leading to an overall ferromagnetic interaction between conduction band electrons and Mn electronic spin. Confirming this, $N_0\alpha = 0.22 \pm 0.01$ eV was measured [13].

The deduction is a bit harder to work out in the valence band. Valence electrons p orbital are not orthogonal to Mn electrons d orbital, meaning there is a competition between the ferromagnetic Coulomb interaction and the anti-ferromagnetic hybridization. However, the hybridization is usually stronger than Coulomb interaction for Mn in II-VI semiconductor, leading to an overall anti-ferromagnetic interaction between holes and Mn electronic spin [14]. For $Cd_xMn_{1-x}Te$, $N_0\beta = -0.88 \pm 0.01$ eV was measured, confirming this tendency [13].

Cr in CdTe

For the Cr, we will rewrite the hamiltonian the exchange interaction in the valence band I_{pd} as I_{hCr} and I_{sd} in the conduction band as I_{eCr}, since we look at the interaction between an exciton and the Chromium atom. The hamiltonian I.73 is the rewrited:

$$\begin{aligned} \mathcal{H}_{DMS,Cr} &= \mathcal{H}_0 & + & \mathcal{H}_{eCr} & + & \mathcal{H}_{hCr} \\ &= \mathcal{H}_0 & + & I_{eCr}\boldsymbol{\sigma}.\mathbf{S} & + & I_{hCr}\mathbf{J}.\mathbf{S} \end{aligned} \tag{I.80}$$

For conduction band electrons, the situation is the same as with the Mn: the s orbital are orthogonal to the Chromium d orbital, and the hybridization is then null. Hence, only Coulomb interaction remain and induce a ferromagnetic coupling between the electrons of the band and the Cr electronic spin. $N_0\alpha$ was never measured in $Cd_xCr_{1-x}Te$, but most most magnetic atoms in II-VI semiconductor presents a value between 0.2 eV and 0.3 eV. It is then generally assume that, in II-VI semiconductor, $N_0\alpha \approx 0.2$ eV [15].

Once again, valence band is a bit more complicated: Coulomb interaction, leading a ferromagnetic coupling, compete with hybridization between valence

band p electrons and Cr d electrons. Direct measure of $N_0\beta$ was neither done in $Cd_xCr_{1-x}Te$, so the competition between these two interactions is difficult to evaluate. Moreover, it has been showed that it was difficult to decide theoretically if the interaction between Cr and holes was ferromagnetic or anti-ferromagnetic both in CdTe and in ZnTe [16]. However, it was found that $N_0\beta$ was positive in $Cd_xCr_{1-x}S$ [17] and in most Zn based II-VI semiconductor, assuming $N_0\alpha = 0.2$ eV [14]. Especially, in ZnTe, still using this assumption, $N_0\beta = +3.6 \pm 1.2$ eV was found [15]. Since there is almost no valence band offset between ZnTe and CdTe, it seems safe to assume that $N_0\beta$ in CdTe is positive and thus the interaction between Cr and holes is ferromagnetic.

I.2.3 Electron-hole exchange in quantum dots

As presented in Sec. I.2.1, electron and hole interact through exchange. Since the recombination of hole and electron in the quantum dot plays an important role in its optical properties, we have to take this new interaction into account to get the full picture. Writing $\mathbf{J} = (J_z, J_+, J_-)$ with $J_+ = J_x + iJ_y$ and $J_- = J_x - iJ_y$, and $\boldsymbol{\sigma} = (\sigma_z, \sigma_+, \sigma_-)$ with $\sigma_+ = \sigma_x + i\sigma_y$ and $\sigma_- = \sigma_x - i\sigma_y$, we can develop the hamiltonian I.55 in a QD symmetry:

$$
\begin{aligned}
\mathcal{H}_{e-h}^{exch} \quad &= 2\delta_0 J_z \sigma_z \quad + \frac{\delta_1}{2}\left(\exp(2i\varphi_1)j_+\sigma_- - \exp(-2i\varphi_1)j_-\sigma_+\right) \\
&\quad + \frac{\delta_2}{2}\left(\exp(2i\varphi_1)j_+\sigma_+ + \exp(-2i\varphi_1)j_-\sigma_-\right)
\end{aligned}
\tag{I.81}
$$

with δ_0 representing the splitting between dark and bright exciton, δ_1 the splitting between the bright exciton states and δ_2 the splitting between the dark exciton states. δ_0 value is controlled both by long-range and short-range interaction, and is typically of about 1 meV in CdTe/ZnTe. δ_1 only appear in anisotropic quantum dot, with φ_1 the direction of the anisotropy, and is induced by the long-range interaction, warying between a few tens and a few hundreds of μeV. Finally, δ_2 primarily arise from the short-range interaction.

Calculating the eigenstate of the hamiltonian I.84, we find the optically active states are linearly polarized along φ_1 and $\varphi_1 + 90°$ as followed:

$$
|\pi_{\varphi_1}\rangle = \frac{1}{\sqrt{2}}\left(\exp(-i\varphi_1)|+1\rangle + \exp(i\varphi_1)|-1\rangle\right)
\tag{I.82}
$$

$$
|\pi_{\varphi_1+90°}\rangle = \frac{1}{\sqrt{2}}\left(\exp(-i\varphi_1)|+1\rangle - \exp(i\varphi_1)|-1\rangle\right)
\tag{I.83}
$$

In order to get the full image of the polarization, the VBM mixing presented in Sec. I.1.4 should also be taken into account. Exchange interaction favours a linear emission along φ_1 and $\varphi_1 + 90°$, while VBM orient the linear emission along θ and

$\theta + 90°$, as presented in Eq. I.49. The competition between these two elements leads to an angle between the two different linearly polarized X lines different from $90°$.

This model works well for quantum dots with an elongated lens shape, in the C_{2v} symmetry. However, more realistic self-assembled quantum dots have symmetries which can deviate quite substantially from the idealized shapes of circular or ellipsoidal lenses. For a C_s symmetry (truncated ellipsoidal lens), additional terms coupling the dark and the bright excitons have to be included in the electron-hole exchange Hamiltonian. Following Ref. [18], the general form of the electron-hole exchange Hamiltonian in the heavy-hole exciton basis $|+1\rangle, |-1\rangle, |+2\rangle, |-2\rangle$ for a low symmetry quantum dot (C_s) is

$$\mathcal{H}_{eh} = \frac{1}{2} \begin{pmatrix} -\delta_0 & e^{-i\pi/2}\delta_1 & e^{i\pi/4}\delta_{11} & -e^{i\pi/4}\delta_{12} \\ e^{i\pi/2}\delta_1 & -\delta_0 & e^{-i\pi/4}\delta_{12} & -e^{-i\pi/4}\delta_{11} \\ e^{-i\pi/4}\delta_{11} & e^{i\pi/4}\delta_{12} & \delta_0 & \delta_2 \\ -e^{-i\pi/4}\delta_{12} & -e^{i\pi/4}\delta_{11} & \delta_2 & \delta_0 \end{pmatrix} \quad (I.84)$$

I.3 Fine and hyperfine structure of a magnetic atom in II-VI semiconductor

I.3.1 Cr atom in II-VI semiconductor

Cr atoms are incorporated into II-VI semiconductors as Cr^{2+} ions on cation sites forming a deep impurity level. This isotope presents *no nuclear spin*, meaning we don't have to consider the hyperfine structure of a Cr atom in a II-VI semiconductor. The ground state of a free Cr^{2+} is ^5D with the orbital quantum number L=2 and a spin S=2 yielding a 25-fold degeneracy. In the crystal field of T_d symmetry of the tetrahedral cation site in zinc-blende crystal, the degeneracy is partially lifted (see Fig. I.3.1): the ^5D term splits into 15-fold degenerate orbital triplet $^5T_2$ and 10-fold degenerate orbital doublet ^5E. The substitution of the Cd atom by a Cr atom lead to a Jahn-Teller distortion of the tetragonal matrix [19]. This distortion reduces the symmetry to D_{2d} and leads to a splitting of the $^5T_2$ ground state into a 5-fold degenerate $^5B_2$ orbital singlet and a ^5E orbital doublet.

The ground state orbital singlet $^5B_2$ is further split by the spin-orbit interaction. In a strain free crystal, it was found that the ground state splitting can be described by the spin effective Hamiltonian [20]:

$$\mathcal{H}_{Cr,CF} = D_0 S_z^2 + \frac{1}{180}F[35S_z^2 - 30S(S+1)S_z^2 + 25S_z^2] + \frac{1}{6}a[S_1^4 + S_2^4 + S_3^4] \quad (I.85)$$

with the Cr spin S=2 and $|D_0| \gg |a|, |F|$. In the model presented here, we use $a = 0$ and $F = 0$. The x, y, z principal axes were found to coincide with the cubic axes (1,2,3) giving rise to three identical sites, each given by I.85 but with the z axis of each along a different cubic axis (1,2,3). A value of $D_0 \approx +30 \mu eV$ was estimated from Electron Paramagnetic Resonance (EPR) measurements in highly diluted bulk (Cd,Cr)Te [20].
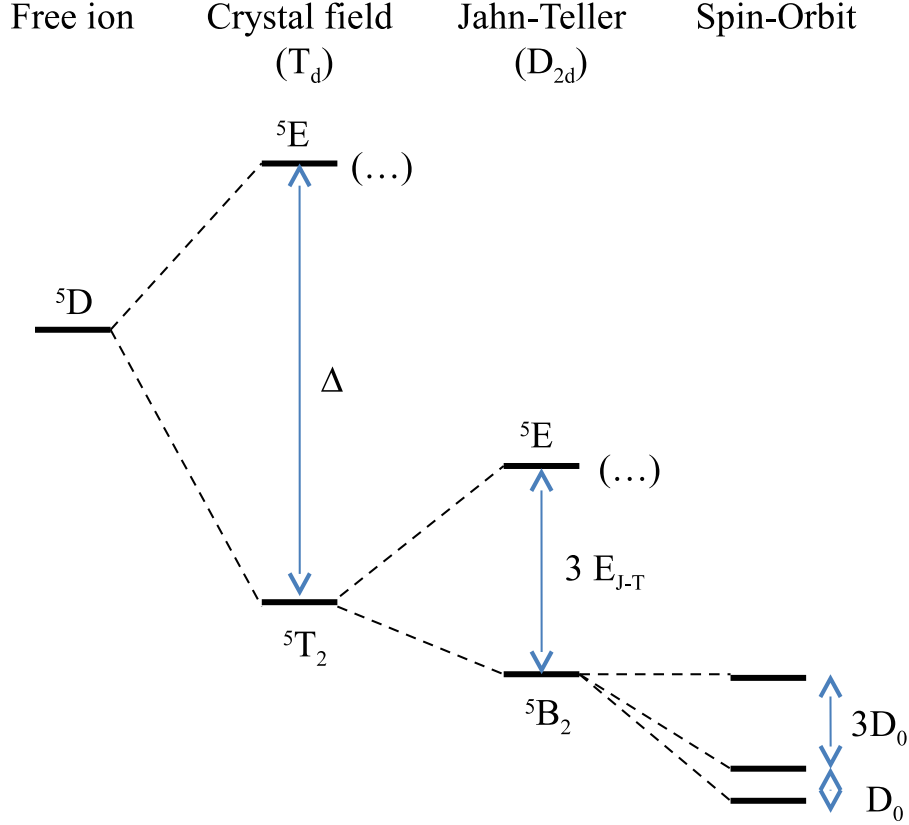

Figure I.7: Scheme of the energy level splitting of Cr^{2+} at a cation site in II-VI compounds having zinc blende structure (T_d) with a crystal field parameter Δ, a Jahn-Teller energy E_{J-T} and a spin-orbit level spacing D_0.

Static biaxial compressive strain in the (001) plane, as observed in self-assembled quantum dots, reduces the symmetry to D_{2d} and destabilize the Cr $3d$ orbitals d_{xz} and d_{yz} having an electron density pointing along the [001] axis (z axis). The Cr ground state is then a 5-fold degenerated orbital singlet formed from the d_{xy} orbital. It corresponds to the Jahn-Teller ground state with a tetragonal distortion along the [001] axis [21].

An applied stress will also influence the Cr spin fine structure splitting through the modification of the crystal field and the spin-orbit interaction [20]. For an arbitrary strain tensor, the general form of the Cr ground state spin effective Hamiltonian is

$$\mathcal{H}_{Cr,\varepsilon} = c_1 e_A S_\theta + c_2 e_\theta S_\theta + c_3 e_\epsilon S_\epsilon + c_4 e_\zeta S_\zeta + c_5(e_\xi S_\xi + e_\eta S_\eta) \qquad (\text{I.86})$$

with S_i defined as:

$$\begin{aligned}
S_\theta &= S_z^2 - \frac{1}{2}[S_x^2 + S_y^2] \\
S_\epsilon &= \frac{1}{2}\sqrt{3}[S_x^2 - S_y^2] \\
S_\xi &= S_y S_z + S_z S_y \\
S_\eta &= S_x S_z + S_z S_x \\
S_\zeta &= S_x S_y + S_y S_x
\end{aligned} \qquad (\text{I.87})$$

and e_i defined similarly as:

$$\begin{aligned}
e_\theta &= \varepsilon_{zz} - \frac{1}{2}[\varepsilon_{xx} + \varepsilon_{yy}] \\
e_\epsilon &= \frac{1}{2}\sqrt{3}[\varepsilon_{xx} - \varepsilon_{yy}] \\
e_\xi &= \varepsilon_{yz} + \varepsilon_{zy} \\
e_\eta &= \varepsilon_{xz} + \varepsilon_{zx} \\
e_\zeta &= \varepsilon_{xy} + \varepsilon_{yx} \\
e_A &= \varepsilon_{xx} + \varepsilon_{yy} + \varepsilon_{zz}
\end{aligned} \qquad (\text{I.88})$$

As shown in Sec. I.1.2, we can write for a flat self-assembled quantum dots with dominant large biaxial strain:

$$\varepsilon_{xx} = \varepsilon_{yy} = \varepsilon_{\parallel}$$
$$\varepsilon_{zz} = -2\frac{C_{11}}{C_{12}}\varepsilon_{\parallel}$$

where $C_{11} \approx 5.4 \ 10^{10} Pa$ and $C_{12} \approx 3.7 \ 10^{10} Pa$ are the elastic constants of CdTe [22]. For this strain configuration, the Cr fine structure is controlled by the spin-lattice coupling coefficients c_1 (symmetric coefficient) and c_2 (tetragonal coefficients). Strain-coupling coefficients estimated from EPR measurements in bulk Cr doped CdTe are listed in table I.2.

We can now simplify the hamiltonian I.86, first reducing it to the active term in our case:

$$\mathcal{H}_{Cr,\varepsilon} = c_1 e_A S_\theta + c_2 e_\theta + S_\theta$$

Table I.2: Values for spin to strain coupling coefficients of Cr in bulk CdTe (in *meV*) extracted from ref. [20].

c_1	c_2	c_3	c_4	c_5
-0.25±2	+4.9 ±2	-1.25±0.5	+4.9±2	+3.7±1.25

Replacing now e_A, e_θ and S_θ by their value given in I.87 and I.88, and using the equalities given in Sec. I.1.2, we can rewrite the strain controlled part of the spin Hamiltonian as $\mathcal{H}_{Cr,\varepsilon}$, depending only on $\varepsilon_\parallel$:

$$
\begin{aligned}
\mathcal{H}_{Cr,\varepsilon_\parallel} &= \underbrace{\frac{3}{2}\varepsilon_\parallel[2c_1(1 - \frac{C_{12}}{C_{11}}) - c_2(1 + 2\frac{C_{12}}{C_{11}})]}_{D_0} \quad S_z^2 \\
&= \qquad\qquad\qquad D_0 \qquad\qquad\qquad\qquad S_z^2
\end{aligned}
\tag{I.89}
$$

where we can estimate $D_0 \approx 1\pm0.6$ meV from the values of the spin-strain coupling coefficients in CdTe (table I.2). However one should note the quantum dots could be partially relaxed and may contain a significant amount of Zn. We were not able to find spin to strain coupling coefficients for Cr in ZnTe and (Cd,Zn)Te alloy in literature. A value of $D_0 \approx +280\mu$eV, much larger than for CdTe, was however estimated in strain-free Cr-doped bulk ZnTe [20]. Larger spin-strain coupling coefficients could then expected for Cr in ZnTe and (Cd,Zn)Te alloys.

Finally, an anisotropy of the strain in the quantum dot plane (001) with principal axis along [010] or [100] axes ($\varepsilon_{xx} \neq \varepsilon_{yy}$ and $\varepsilon_{xy}=\varepsilon_{yx}=0$) would affect the Cr fine structure through the tetragonal coefficient c_3. This coupling can be described by an additional term in the spin-strain Hamiltonian

$$
\begin{aligned}
\mathcal{H}_{Cr,\varepsilon_\perp} &= \underbrace{\frac{3}{4}c_3(\varepsilon_{xx} - \varepsilon_{yy})}_{E} \quad (S_x^2 - S_y^2) \\
&= \qquad\quad E \qquad\qquad (S_x^2 - S_y^2)
\end{aligned}
\tag{I.90}
$$

This anisotropy term E couples Cr spin states separated by two units and in particular $S_z=+1$ to $S_z=-1$ which are initially degenerated. It could be exploited to induce a large strain mediated coherent coupling between a mechanical oscillator and the Cr spin [23].

We can now group I.89 and I.90 in order to write the complete hamiltonian of anisolated Cr in a strained, anisotropic CdTe/ZnTe quantum dot:

$$
\begin{aligned}
\mathcal{H}_{Cr,\varepsilon} &= \mathcal{H}_{Cr,\varepsilon_\parallel} + \mathcal{H}_{Cr,\varepsilon_\perp} \\
&= D_0 S_z^2 + E(S_x^2 - S_y^2)
\end{aligned}
\tag{I.91}
$$

Chapter II

Magneto-optical study of Cr-doped CdTe quantum dots

In this chapter, we will study the photoluminescence of a II-VI quantum dot containing a single Chromium atom. We saw in the chap. I.3.1 that the magnetic anisotropy of the spin lead to a zero magnetic field splitting of the 0, ± 1 and ± 2 states. In a neutral Cr-doped quantum dot, such an anisotropy is induced by the bi-axial strains in the plane of the dots. Probing optically the dot, it results that exchange interaction is enough to see the effect of the presence of a single Cr spin in the QD. Studying the magnetic-field dependence of the quantum dots photoluminescence, we will also show the influence of the symmetry on carrier-Cr spin coupling.

II.1 Strained quantum dots containing an individual Cr atom

II.1.1 Energy structure of a Cr in a quantum dot

Using the procedure described in the chap. **??**, we randomly incorporated Cr atom in CdTe/ZnTe quantum dots, adjusting the density of the Cr atoms to be roughly equal to the density of dots, in order to get QDs containing 0, 1 or a few Cr atoms. The photoluminescence (PL) of individual QDs, induced by optical excitation with a dye laser tuned on resonance with an excited state of the dots, is studied by optical micro-spectroscopy.

Low temperature (T=5K) PL of the neutral exciton (X-Cr) of several QD doped with a single Cr are reported in Fig. II.1. Four emission lines are observed as shown in QD3, with the central peak being split in some QDs, such as QD1 and QD2 spectra. Scanning with an energy tunable laser, we saw that all the peaks
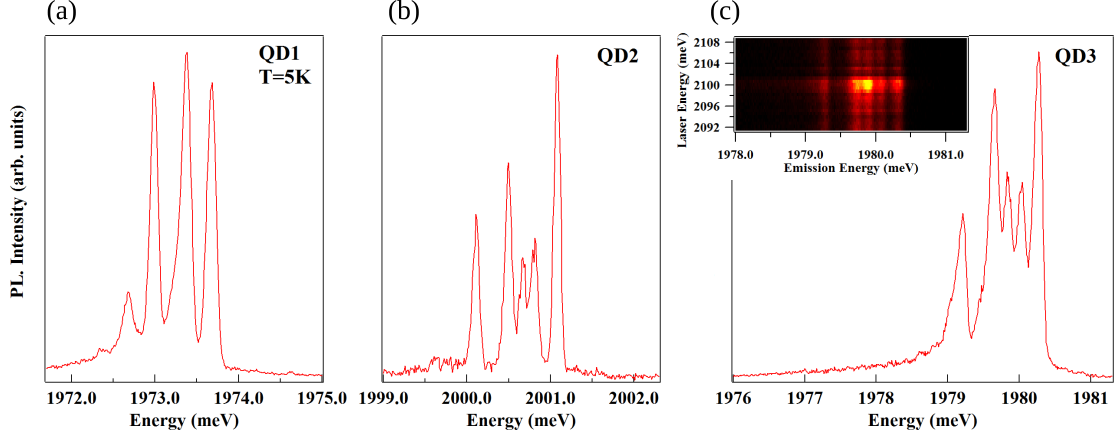
Figure II.1: (a) PL of QD1 X-Cr complex at low temperature (T=5K). Inset presents the PLE map of this QD, showing a sharp quasi-resonant state for an excitation at 2100 meV. (b) PL of QD2 X-Cr complex at low temperature. (c) PL of QD3 X-Cr complex at low temperature.

share a common quasi-resonant state, where all are at a maximum intensity, as highlighted in the inset of Fig. II.1(a). This is an indication that they originate from the same dot. Variations in the relative intensities of the peaks are observed in different dots. The lowest energy peak is shown as getting more intense when the splitting of the central peak get wider.

In a II-VI semiconductor, the orbital momentum of the Cr connects the spin of the atom to its local strain environment through the modification of the crystal field and the spin-orbit coupling. For biaxial strain in the (001) plane, the ground state of a Cr spin is split by a strain induced magnetic anisotropy term $\mathcal{H}_{Cr,\varepsilon_\parallel} = D_0 S_z^2$ (see chap. I.3.1). It was deduced from electron paramagnetic resonance of bulk Cr-doped CdTe that D_0 is positive for compressive biaxial strain [19]. In a self-assembled CdTe/ZnTe QD with large in-plane strain, the Cr spin energy levels are split with S_z=0 at low energy (Fig. II.2). A value of D_0 in the 1 meV range can be expected for a CdTe layer strained on a ZnTe substrate, as shown in chap. I.3.1.

When an electron-hole (e-h) pair is injected in a Cr-doped QD, the bright excitons are split by the exchange interaction between the spins of Cr and carriers. In flat self-assembled QDs, the heavy-holes and light-holes are separated in energy by the biaxial strain and the confinement. In a first approximation, the ground state in such QD is a pure heavy-hole ($J_z=\pm3/2$) exciton and the exchange interaction with the Cr spin S is described by the spin Hamiltonian

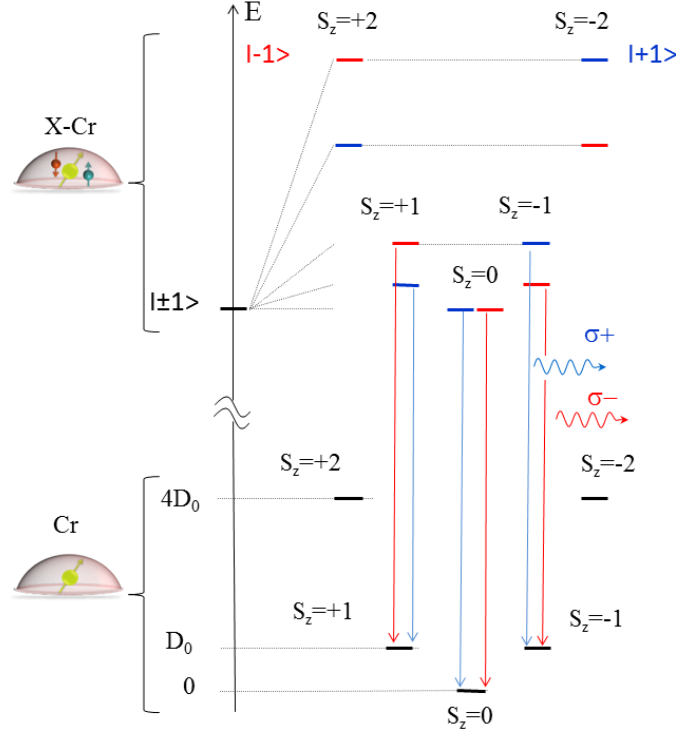$$\mathcal{H}_{c-Cr} = I_{eCr}\vec{S}\cdot\vec{\sigma} + I_{hCr}S_z J_z \tag{II.1}$$

Figure II.2: Illustration of the energy levels of the ground state (Cr), the bright exciton states ($|\pm 1\rangle$) coupled to the spin of a Cr (X-Cr) and dominant PL transitions ($\sigma+$, σ-). The states $|S_z = \pm 2\rangle$ cannot be populated through thermalization, and thus the recombination channel are not shown on this schema.

with $\vec{\sigma}$ the electron spin and J_z the hole spin operator. I_{eCr} and I_{hCr} are, respectively, the exchange integrals of the electron and the hole spins with the Cr spin. These exchange energies depend on the exchange constant of the $3d$ electrons of the Cr with the carriers in CdTe and on the overlap of the Cr atom with the confined carriers. The exchange interaction of the Cr spin is ferromagnetic for both electron and hole spins in common II-VI semiconductors and a typical exchange constant 4 to 5 times larger for the holes than for the electrons is also expected in CdTe [24, 25].

For highly strained CdTe/ZnTe QDs with a weak hole confinement, the strain induced energy splitting of the Cr spin $D_0 S_z^2$ is much larger than the exchange energy with the confined carriers ($D_0 \gg |I_{hCr}| > |I_{eCr}|$). The exchange interaction with the exciton acts as an effective magnetic field which further splits the Cr spins states $S_z = \pm 1$ and $S_z = \pm 2$. The resulting X-Cr energy levels are presented in Fig. II.2. The exciton recombination does not affect the Cr atom and its spin

33

is conserved during the optical transitions. Consequently, the large strain induced splitting of the Cr spin is not directly observed in the optical spectra. However, at low temperature, the Cr spin thermalize on the low energy states $S_z=0$ and $S_z=\pm1$. This leads to a PL dominated by three contributions: a central line corresponding to $S_z=0$ and the two outer lines associated with $S_z=\pm1$ split by the exchange interaction with the carriers.
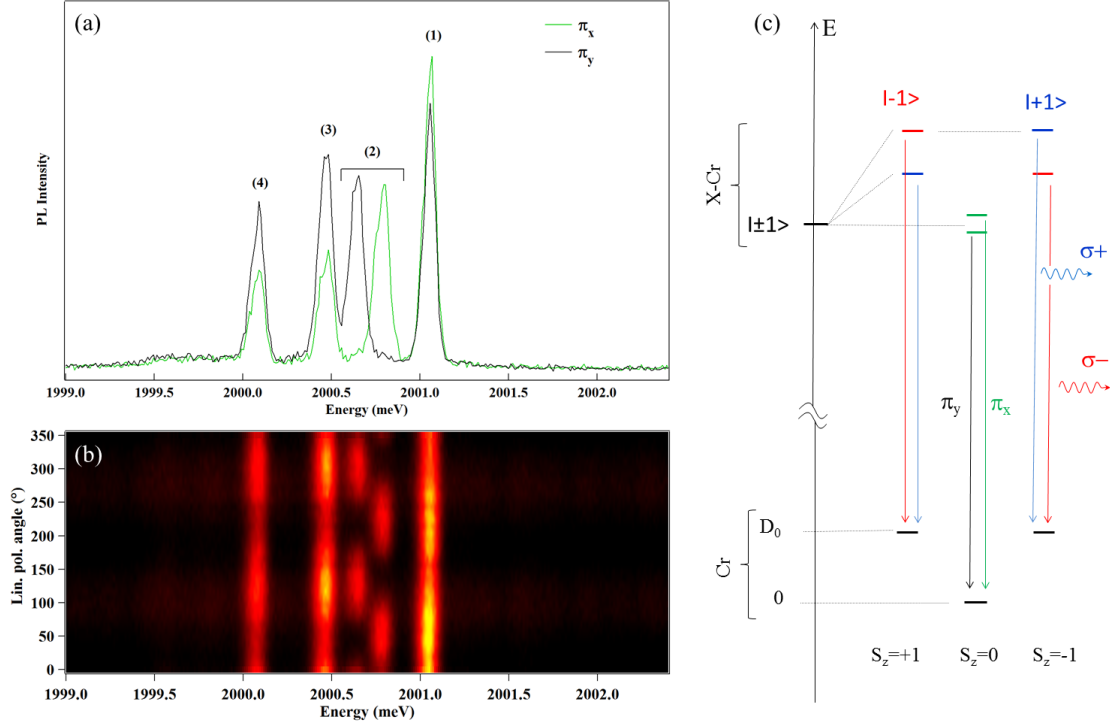

Figure II.3: (a) Low temperature (T=5K) PL of QD2 recorded in circular polarization: $\sigma+$ in blue and $\sigma-$ in red. (b) Low temperature PL of QD2 recorded along two orthogonal directions. (c) Linear polarization PL intensity map of QD2. The $0°$ polarization angle corresponds to an emission polarized along the QD cleavage axis, either 110 or $1\bar{1}0$. (d) Illustration of the energy levels of the ground state (Cr), the bright exciton states ($|\pm1\rangle$) coupled to the spin of a Cr (X-Cr), showing the splitting of the central peak via the bright exciton coupling, and dominant PL transitions ($\sigma+$ (blue), $\sigma-$ (red) and π (green and black)).

Cr-doped quantum dots exhibit a linear polarization dependence, as presented in Fig. II.3. The central line ($S_z=0$) is split and linearly polarized along two orthogonal directions. As in non-magnetic QDs, this results from a coupling of the two bright excitons $|\pm1\rangle$ by (i) the short range e-h exchange interaction

34

in the presence of valence band mixing and/or (ii) the long-range e-h exchange interaction in a QD with an in-plane shape anisotropy [26]. This anisotropic e-h exchange energy mixes the bright exciton associated with the same Cr spin state, inducing an extra splitting between them. The mixing is maximum for the central pair of bright excitons (S_z=0) which are initially degenerated. The outer lines are also slightly linearly polarized but the influence of the e-h exchange interaction is attenuated by the initial splitting of the $|\pm 1\rangle$ excitons induced by the exchange interaction with the Cr spin S_z=± 1.
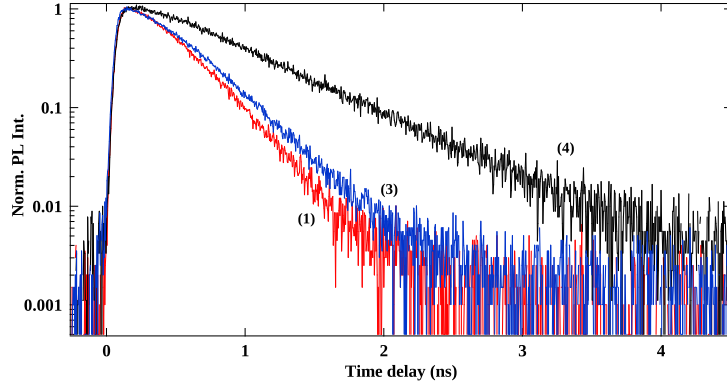
Figure II.4: Time resolved PL of QD2 taken on two exterior peaks, attributed to $|S_z = +1\rangle$ and $|S_z = -1\rangle$ (noted (1) and (3) in Fig. II.3(a)), and the lower energy one (noted (4)).

In order to identify the lower energy peak ((4) in Fig. II.3(a)), we took the time resolved photoluminescence of the emission peaks, presented in Fig. II.4. One can notice that the line (4) present a decay time about twice as long as the high energy peak. A long recombination time is one of the characteristics of a dark exciton emission [27]. Under normal circumstances, the recombination of such a state is non-radiative. However, it is possible to observe a dark exciton recombination emitting a photon in low symmetry quantum dot [28]. This hypothesis will be confirmed by the magneto-optical study of the dot presented in Fig. II.8 and II.10.

Since the absence of PL on $|\pm 2\rangle$ is linked to their impossibility to be thermally populated, one could expect to see their emission at higher temperature. Fig. II.5 presents the dot PL at several temperatures. With the increase of the temperature, we observe a significant line broadening induced by the interaction with acoustic phonons. In order to keep a significant PL intensity and resolved PL lines, we limited our investigation to temperature below 50K. No contribution of the $|S_z$=$\pm 2\rangle$ Cr spins states are observed in the emission of the exciton.
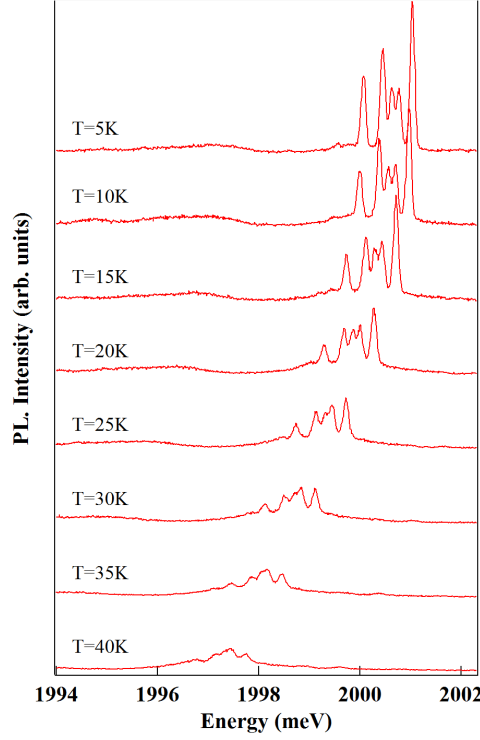
Figure II.5: Temperature evolution of QD2 PL, from T=5K to T=40K. The red shift and peak broadening are clearly visible. Even at 40K, $|S_z = \pm 2\rangle$ states do not appear.

II.1.2   Excited states of a Cr-doped QD

In order to study the different excited states presented by a QD doped with a single Cr atom, we took the PLE of QD2 starting close the dot. The dot spectra is presented in Fig. II.6(a) in both σ polarizations. The central peaks do not show dependency in circular polarization, which is coherent with their linear polarization dependency presented in Fig. II.3(a) and (b). The excitation laser is $\sigma+$ polarized in order to control the spin of the injected exciton. The exterior peaks emission being in $\sigma+$ polarization shows that there is no spin flip of the exciton before recombination.

Fig. II.7(a) presents the entire PLE of QD2 X-Cr complex. However, one can note several other excited states along the scan. In this section, we will discuss several of them.

The first remarkable feature of this scan is the really long luminescence of the acoustic phonon replica. As shown on the zoom in Fig. II.7(b), the probed peak
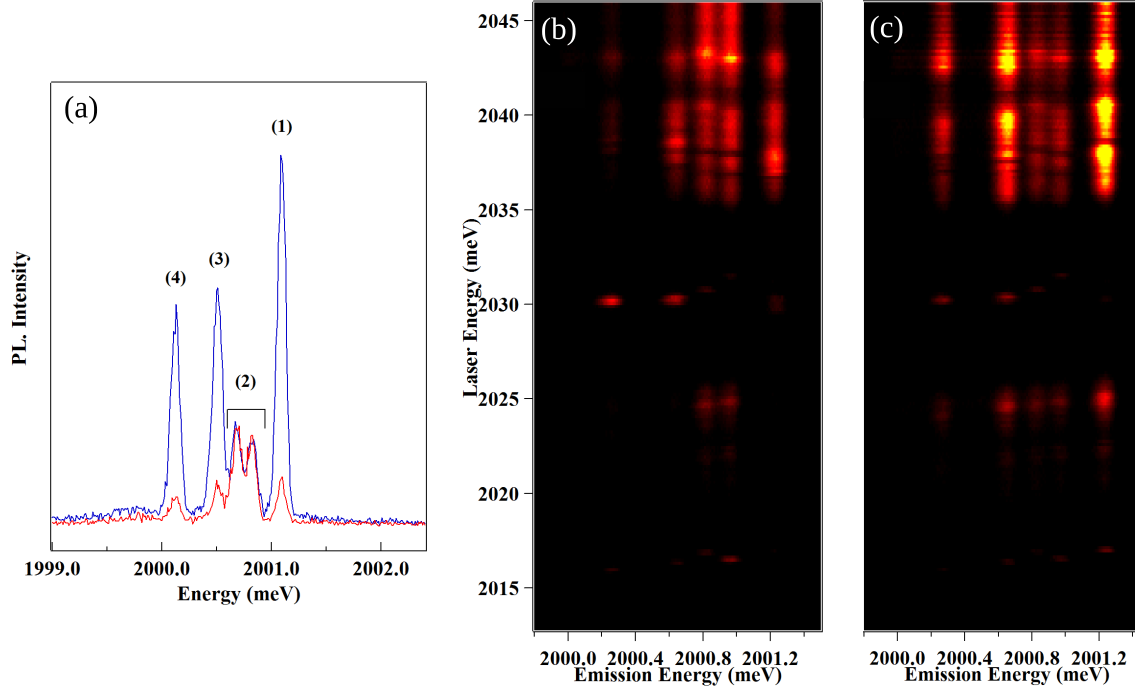
Figure II.6: (a) PL spectra of the exciton in QD2 (X-Cr) for co-circularly (blue) and cross-circularly (red) polarized excitation/detection [À VÉRFIER : taken on the 2175 meV quasi-resonant state]. (b) - (c) PLE map between 2046 meV and 2013 meV presenting several excited, detecting in σ_{co} (b) and σ_{cross} (c).

continues to emit with an excitation several millielectronvolt above the excited state, remaining visible until 2004 meV. One can also see two sharp intensity diminutions in this emission. Mapping the intensity of this peak emission to the quantum dot spectrum (Fig. II.7(c)), it is evidenced that these diminutions occur when the laser is in resonance with a QD emission line. The absorption then preferentially occurs in this resonantly excited state than in the acoustic phonon band.

At higher excitation energy, several excited states appear. The lower energy one is around 2018.5 meV, zoomed in on Fig. II.7(e). On this excited state, each peak presents a slightly different resonant energy. One can see that the order of appearance of the two central peaks seems to be reversed compared to the external ones. This phenomenon was first observed on QDs in GaAs quantum well [29]. This indicates an inversion of the splitting due to electron-hole exchange interaction [26].

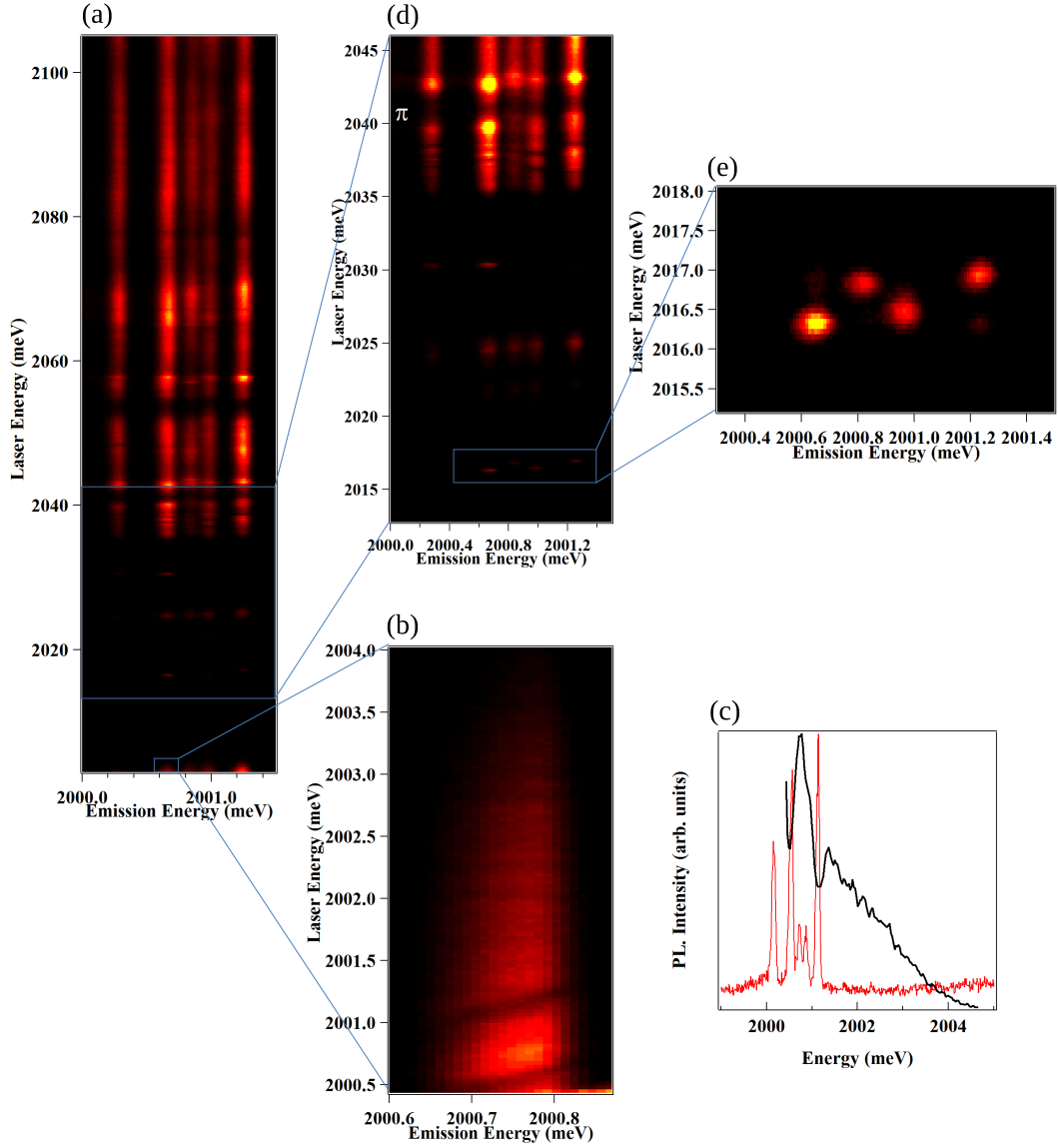Another excited state can be saw at 2025 meV. This excited state occurs on a

Figure II.7: (a) QD2 X-Cr PLE map in σ_{cross} polarization. Several excited states are highlighted. (b) PLE scan of the lower energy peak, taken close to the QD emission energy, showing the phonon replica taken in π detection. The emission integrated intensity in function of the laser energy is plotted in (c) (black curve) along with the PL spectra of QD2 taken in σ_{co} polarization. (d) PLE map between 2046 meV and 2013 meV presenting several excited, detecting in π. (d) Zoom in a particular excited state presented a splitting inversion, taken in π detection.

38

large energy band and can be linked back to an excitation to the optical phonon. Looking at the σ polarized emission of this state (Fig. II.6(b) and (c)), we can see that this excitation presents a really good spin conservation: the low and high energy peaks are strongly σ polarized, while the central peaks do not show dependency over circular polarization. This, once again, show the good spin conservation of the system, as highlighted on the quasi-resonant state.

Finally, another interesting excited state appear at 2030 meV. This state presents an exchange-induced splitting different from the splitting in the quasi-resonant state. This is due to a difference in the carriers and Cr atom wavefunction overlap. One can also noticed the this state presents a stronger luminescence in σ_{cross} than in σ_{co}, [TO REDISCUSS] hinting at a spin flip of the hole before the recombination.

II.1.3 Magneto-optics of a quantum dot doped with a single Cr

The structure of the energy levels in Cr-doped QDs is confirmed by the evolution of the PL spectra in magnetic field (up to 11T) in Faraday configuration [30], presented in Fig. II.8. One can see that the Zeeman energy of the exciton under magnetic field can compensate the exciton splitting induced by the exchange interaction with the Cr [31]. For QD3, this results in an anti-crossing of $|+1\rangle$ and $|-1\rangle$ excitons due to the e-h exchange interaction around B_z=6 T observed both in $\sigma+$ and $\sigma-$ polarizations (anti-crossing (2) and (3) in Fig. II.8(a)).

The low energy emission presented as a dark exciton in Fig. II.4 shows an anti-crossing with the bright excitons under B_z in $\sigma-$ polarization (anti-crossing (4) in Fig. II.8). As illustrated in Fig. II.10(b), this anti-crossing arises from a mixing of the bright and dark excitons interacting with the same Cr spin state. Observed in $\sigma-$ polarization, it corresponds to the mixing of the exciton states $|-1\rangle$ and $|+2\rangle$ coupled to the Cr spin S_z=-1. This dark/bright excitons coupling δ_{12} is induced by the e-h exchange interaction in a confining potential of reduced symmetry (lower than C_{2v}) [32]. In such symmetry, the dark exciton acquire an in-plane dipole moment which lead to possible optical recombination at zero magnetic field [28] as observed in these QDs. The oscillator strength of this "dark exciton" increases as the initial splitting between $|-1\rangle$ and $|+2\rangle$ excitons is reduced by the magnetic field (Fig. II.10(b)).

To illustrate the influence of the QD symmetry on the magneto-optical properties of X-Cr, we show in Fig. II.9(b) the emission of a QD with a different strain state (QD4). For QD3, the splitting of the central peak is not clear in the PL at 0T (Fig. II.1(a)) without the linear polarization map, while two linearly polarized peaks appears clearly in QD4 spectra. This difference in emission arise from a
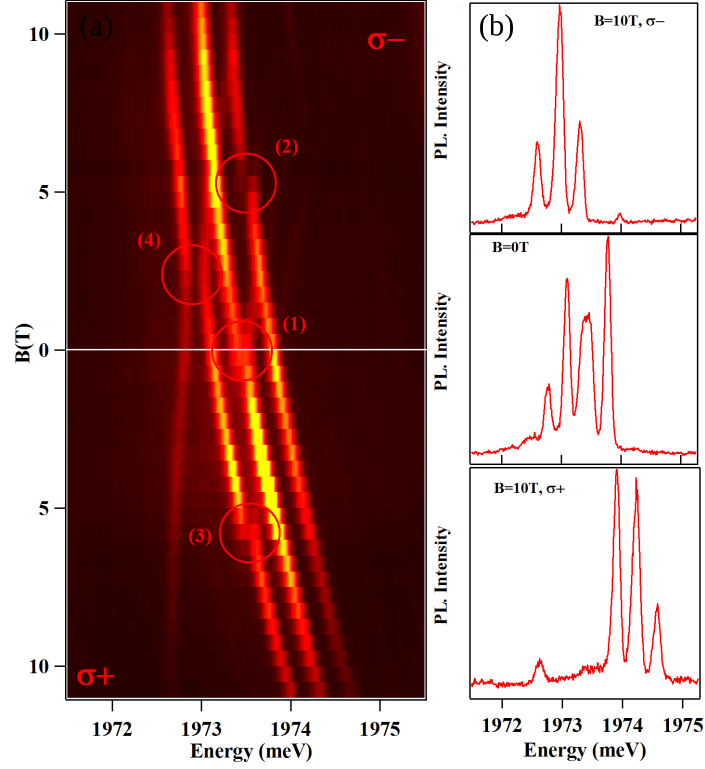
Figure II.8: (a) Circularly polarized X-Cr PL evolution under magnetic field (B_z) in QD1. Noticeable anti-crossing are highlighted and numbered. (b) QD1 X-Cr PL spectra taken at 0 and ±10T.

difference in the in-plane strain of each QD [26]. The dark exciton emission is also stronger in QD2, confirming a lower symmetry than QD3.

Investigating both the biexciton and the exciton in the same Cr-doped QD, we can also analyze the impact of the carrier-Cr interaction on the fine structure of the Cr spin. The magnetic field dependency of X^2-Cr emission in QD2 is presented along with the X-Cr emission as a contour plot in Fig. II.9(a) and (b) respectively. The PL under magnetic field of X-Cr and X^2-Cr present a mirror symmetry. In particular, the dark/bright exciton mixing observed around B_z=2.5T on the low energy side of the PL in $\sigma-$ polarization for X-Cr is observed on the high energy side in $\sigma+$ polarization for X^2-Cr (circles in Fig. II.9(a) and (b)).

If one consider the ground state of X^2 as a spin-singlet (total spin 0), it cannot be split by the magnetic field or the spin interaction part of the carriers-Cr Hamiltonian. The creation of two excitons in the QD cancels the exchange interaction with the Cr atom. Thus, the PL of X^2-Cr is controlled by the final state of the
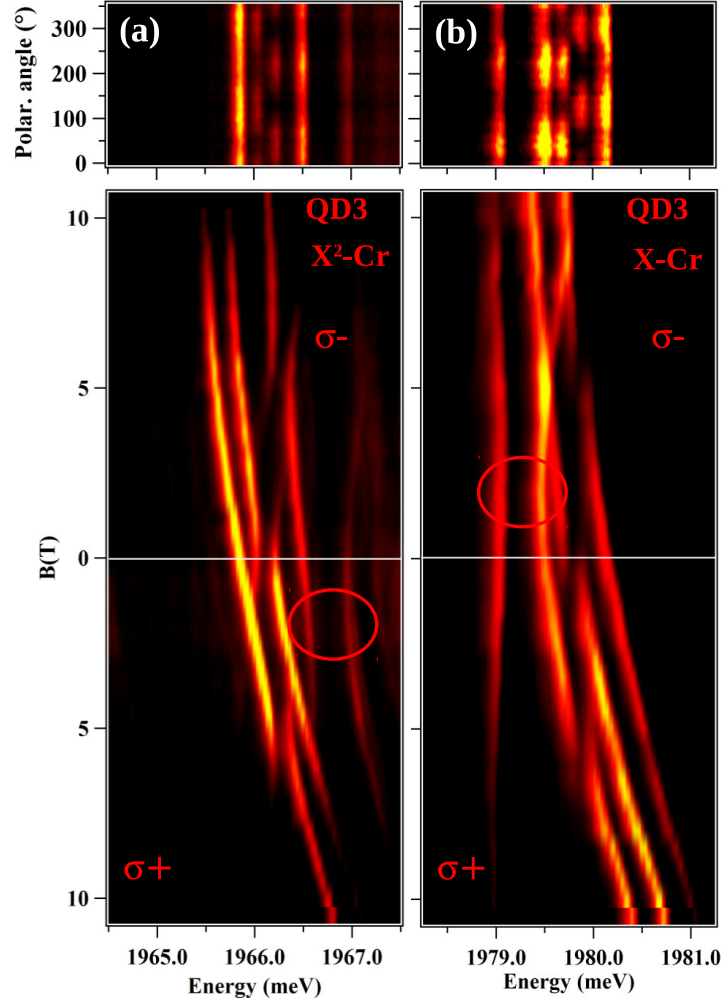
40

Figure II.9: Linear polarization intensity map (top panel) and intensity map of the longitudinal magnetic field dependence of the emission (bottom panel) of (a) X^2-Cr and (b) X-Cr in QD3.

optical transitions, i.e. the eigenstates of X-Cr, resulting in the observed mirror symmetry in the PL spectra. However, in some of the QDs, the X^2-Cr emission slightly deviates from this simple picture: a smaller energy splitting is observed for X^2-Cr compared to X-Cr (see X-Cr and X^2-Cr in Fig. II.9). This shows that there is an interaction of X^2 with the Cr atom. It could result from a perturbation of the carriers' wave function by the interaction with the magnetic atom [33, 34] or a modification the local electric field which controls the Cr fine structure. [TO
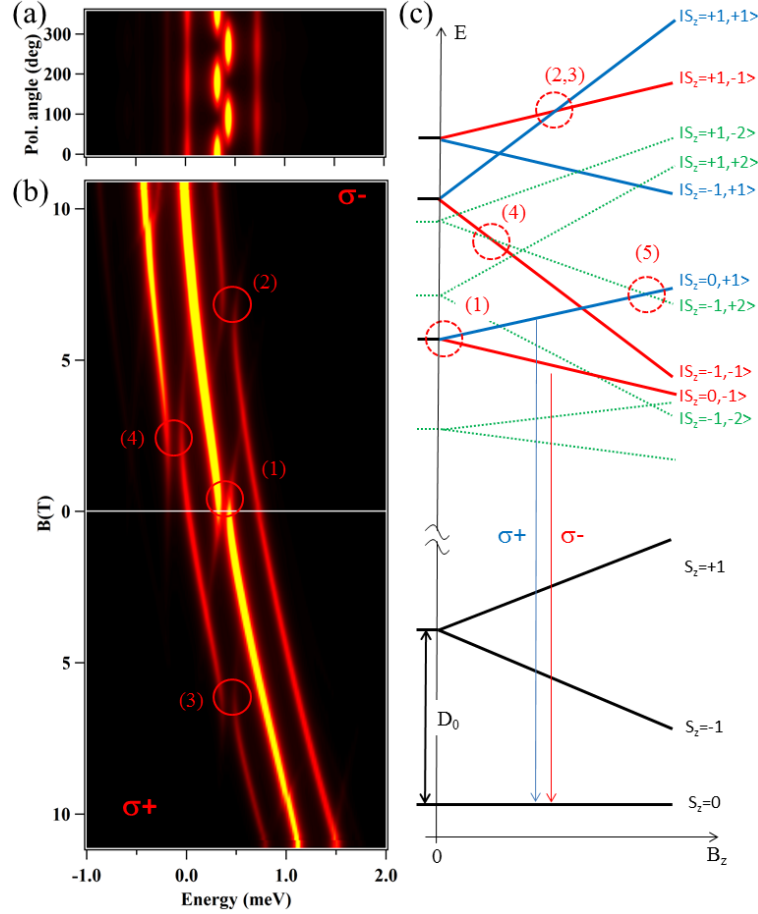
41

II.2 Modelization of a Cr-doped QD

Figure II.10: (a) Up: Calculated linear polarization PL intensity map of X-Cr at zero field. The 0° polarization angle correspond to an emission polarized along the 100 axis. Down: Calculated X-Cr circularly polarized magnetic field dependency. Details of the model and parameters are listed in Tab. II.1. Corresponding anti-crossing are highlighted in same fashion as on Fig. II.8. (b) Schema of the magnetic field dependency of the energy levels of the low energy Cr spin states $S_z=0$ and $S_z=\pm1$, and corresponding bright ($|+1\rangle$ blue, $|-1\rangle$ red) and dark ($|\pm2\rangle$ green) X-Cr energy levels.

We calculated the magneto-optic behaviour of Cr-doped QDs by diagonalizing

the complete Hamiltonian of the e-h-Cr in self-assembled dots. This hamiltonian can be separated as follows:

$$\mathcal{H}_{X-Cr} = \mathcal{H}_{Cr,\varepsilon} + \mathcal{H}_{cCr} + \mathcal{H}_{mag} + \mathcal{H}_{eh} + \mathcal{H}_{band} + \mathcal{H}_{scat} \tag{II.2}$$

where:

$\mathcal{H}_{Cr,\varepsilon}$ describes the fine structure of the Cr atom and its dependency on local strain, as presented in Eq. I.91. It is mainly drived by D_0, the magnetic anisotropy. E, the in-plane strains, also appears in this Hamiltonian, but have to be kept small in order to model the found dots (see Fig. II.11 for the emission of a dot with a higher E).

$\mathcal{H}_{cCr}$ describes the coupling of the electron and hole with the Cr spin, depending on I_{eCr}, the exchange integral of the electron-Cr spins, and I_{hCr}, the exchange integral of the hole-Cr spins, as described in Eq. I.80.

$\mathcal{H}_{mag}$ describes the effect of an exterior magnetic field, coupled to both the Cr and carrier spins by the Zeeman terms, depending on the g-factor of each of them and the Bohr magneton μ_B, and including the diamagnetic shift of the electron-hole via the term γ.

$$\mathcal{H}_{mag} = g_{Cr}\mu_B \overrightarrow{B}.\overrightarrow{S} + g_e\mu_B \overrightarrow{B}.\overrightarrow{\sigma} + g_h\mu_B \overrightarrow{B}.\overrightarrow{J} + \gamma B^2 \tag{II.3}$$

$\mathcal{H}_{eh}$ describes the short range and long range electron-hole interaction, through the bright and dark exciton splitting δ_0, the bright exciton coupling δ_1, the dark exciton coupling δ_2 and the bright and dark exciton coupling δ_{11} and δ_{12}. All of these term are described in Eq I.84.

$\mathcal{H}_{band}$, the band Hamiltonian, presented in Eq. I.4 and I.8, stands for the energy of the electrons (i.e. the band gap energy E_g), and the heavy-holes (hh) and light-holes (lh) energies, depending on the splitting between lh and hh Δ_{lh}, and the anisotropy of the QD.

$\mathcal{H}_{scat}$ describes the perturbation of the wave function of the exciton in the initial state of the optical transition by the hole-Cr exchange interaction, controlled by the parameter η. This perturbation depends on the value of the exchange energy between the Cr spin S_z and the hole spin J_z and can be represented, using second order perturbation theory, by an effective spin Hamiltonian [33–35]

$$\mathcal{H}_{scat} = -\eta S_z^2 \tag{II.4}$$

with $\eta > 0$.

We considered the general case of QDs with a symmetry lower than C_{2v} (truncated ellipsoidal lens for instance [32]), and took into account the influence of this reduced symmetry on the valence band and on the e-h exchange interaction. The

Table II.1: Values of the parameters used in the model of Cr-doped CdTe/ZnTe quantum dot presented in Fig. II.10. The value of the parameters not listed in the table is 0. The chosen values are typical for CdTe/ZnTe quantum dots and can be compared with parameters extracted from Mn-doped quantum dots [28, 35]. These values are reasonable to reproduce the emission of the QDs presented in this thesis.

| I_{eCr} | I_{hCr} | δ_0 | δ_1 | δ_{12} | δ_{11} | $\frac{|Q|}{\Delta_{lh}}$ | $\frac{|R|}{\Delta_{lh}}$ |
μeV	μeV	meV	μeV	μeV	μeV		
-70	-280	-1	250	150	50	0.05	0.05

| arg(R) | D_0 | g_{Cr} | g_e | g_h | γ | η | T_{eff} |
	meV				$\mu eV/T^2$	μeV	K
$-\frac{\pi}{2}$	2.5	2	-0.7	0.4	1.5	25	25

population of the X-Cr spin states split by the large magnetic anisotropy and the carriers-Cr exchange interaction is described by a spin effective temperature T_{eff}. The results of the model obtained with T_{eff}=25K, D_0=2.5 meV and an electron-Cr (hole-Cr) exchange interaction I_{eCr}=-70μeV (I_{hCr}=-280 μeV) are reported in Fig. II.10 (parameters not specific to Cr-doped QDs are listed in Tab. II.1). Such parameters do not aim to fit the data and are only reasonable order of magnitude. The PL of X-Cr at zero field and its evolution in magnetic field can be qualitatively reproduced. In particular, the description of the spin states occupation by T_{eff} is sufficient to reproduce the observed emission from the three low energy X-Cr levels (Cr spin states S_z=0 and S_z=±1). The splitting of the central line at zero field (anti-crossing (1)) and the anti-crossings under magnetic field (anti-crossings (2) and (3) around B_z=6T for the Cr spin states S_z=+1 and anti-crossings (4) with the dark exciton around B_z=2T) are also well reproduced by the model.

The magnetic anisotropy D_0 cannot be precisely extracted from the PL spectra. However, a higher value would produce a smaller PL intensity of the sates S_z=|±1⟩ than observed experimentally. In addition, for $D_0 < 2.25$ meV, an anti-crossing due to an electron-Cr flip-flop controlled by I_{eCr}, labelled (5) in Fig. II.10(c), would appear below B_z=11T on the central line in σ+ polarization.

Having shown that our model reproduce well the evolution of the emission under variations of different parameters, we can run it to see the influence of E on the emission. This simulation was done by applying a small magnetic anisotropy D_x along the x axis of the quantum dot and none along the y axis (D_y=0), creating an effective E. Results of such a study are presented on Fig. II.11, (a) and (b) for the X-Cr system, and (c) and (d) for the X^c-Cr one.

The X-Cr map in linear polarization presents a dependency on all the three peaks at 0T, when only the central peaks exhibit this behaviour in dots with a
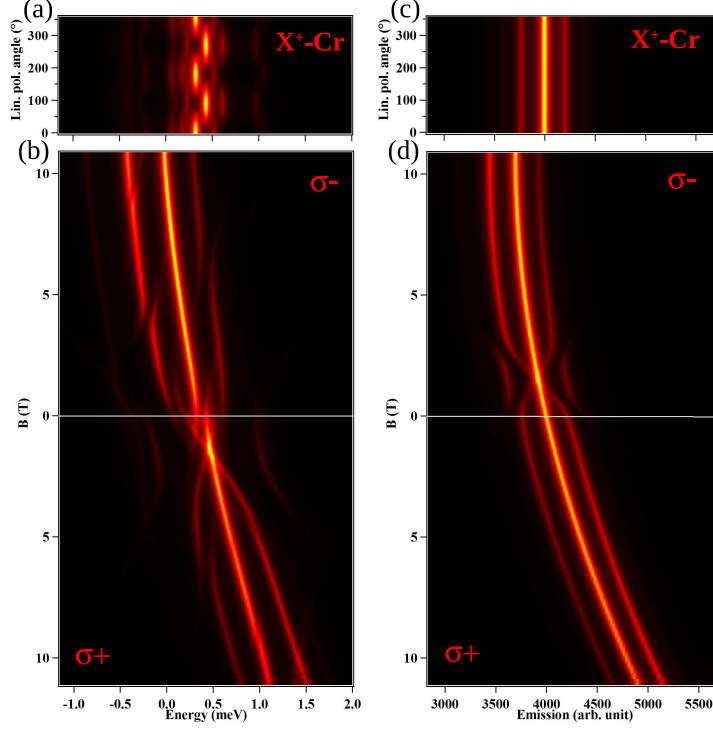
Figure II.11: For a QD with a small magnetic anisotropy along the x axis ($D_x = 150$ μeV, $D_y = 0$ μeV, $D_z = 2500$ μeV): (a) calculated X-Cr linear polarization PL intensity at 0T; (b) calculated X-Cr circularly polarized magnetic field dependency; (c) calculated X^c-Cr linear polarization PL intensity at 0T; and (d) calculated X^c-Cr circularly polarized magnetic field dependency.

small in-plane anisotropy at the Cr position. The effect of such an anisotropy is to coupled to spin levels separated by two spin units, such as $|S_z = -1\rangle$ and $|S_z = +1\rangle$. This induce a mixing between two bright exciton states, leading to a linearly polarized emission. For a low E value, the strain induced splitting of $|S_z = \pm1\rangle$ is high enough to strongly reduce the mixing of the exciton states. A higher in-plane strain anisotropy is able to couple the spin level and induced the linearly polarized emission.

As can be expected, X^c-Cr doesn't present any linear polarization dependency, as shown on Fig. II.11(c).

The evolution of the emission under magnetic field also presents different characteristics than a QD with magnetic anisotropy purely along z. Fig. II.11(b) presents the evolution in B of the X-Cr emission. One can note anti-crossings at +5T appearing on both $|S_z = +1\rangle$ and $|S_z = -1\rangle$, as well as an anti-crossing at

-5T appearing on the low energy emission lines. These are similar to the anti-crossing (2), (3) and (4) on Fig. II.10. Around 0T, other anti-crossings appear, on all the three peaks this time. Anti-crossing on the central peaks is the same as the anti-crossing (1) in Fig. II.10. The ones appearing on the $|S_z = \pm 1\rangle$ peaks arise from the exciton mixing via E, as evidenced by the linear polarization.

X^c-Cr in dot with high in-plane anisotropy at the Cr position also presents anti-crossing for a magnetic field around 1T, as shown in Fig. II.11(d). This anti-crossing appears when the Zeeman effect of the Cr atom compensates the electron-Chromium interaction and the hole-Chromium interaction.

II.3 Charge fluctuation of a Cr ion in the vicinity of the QDs

Some dots were found presenting a linear polarization dependency both on their central peaks and on their exterior peaks. However, such dots didn't present any anti-crossing when probed under magnetic field. Results of these experiments are presented in Fig. II.12.

A common feature of all of these dots is the thin and well split X^+-Cr PL structure, shown on Fig. II.12(a) around 1949mev. X-Cr and X^2-Cr also present three well defined peaks, with a broad emission. This is not a general case, as some dots were found presenting a broad emission on X-Cr and X^2-Cr positions, such as QD6 presented in Fig. II.14. The linear polarization map of the PL of QD4 reveals that each peak presents a linear polarization dependency (Fig. II.12(b) and (c)).

The PL evolution of such a dot is presented in Fig. II.12(d). The diamagnetic shift is clearly visible. However, the only anti-crossings appear at B=9T for all the peaks (zoom in Fig. II.12(d)). Such anti-crossings are characteristic of an exciton in a QD with no magnetic atom: it arise from the dark and bright exciton mixing.

In order to get more informations on these dots, it was decided to study them applying a bias voltage. The application of an electric field was realized via a sample with a Schottky gate in the same fashion than the one in chap. ??. The resulting map is presented in Fig. II.13(a). The first visible feature is the strong electric field dependency of the emission energy, more marked for X-Cr than for the X^c-Cr systems. The emission energy variation of the X-Cr complex occur on a 2.9 meV scale.

There is another remarkable point on these maps, evidenced on the X^+-Cr complex on the Fig. II.13(b): the splitting between each peak is changing with the applied electric field. The splitting between the high and low energy peaks varies from 0 meV for an applied bias voltage of -12V (no splitting) to 0.76 meV for 13V applied. This disappearance of the splitting for a certain bias voltage indicates
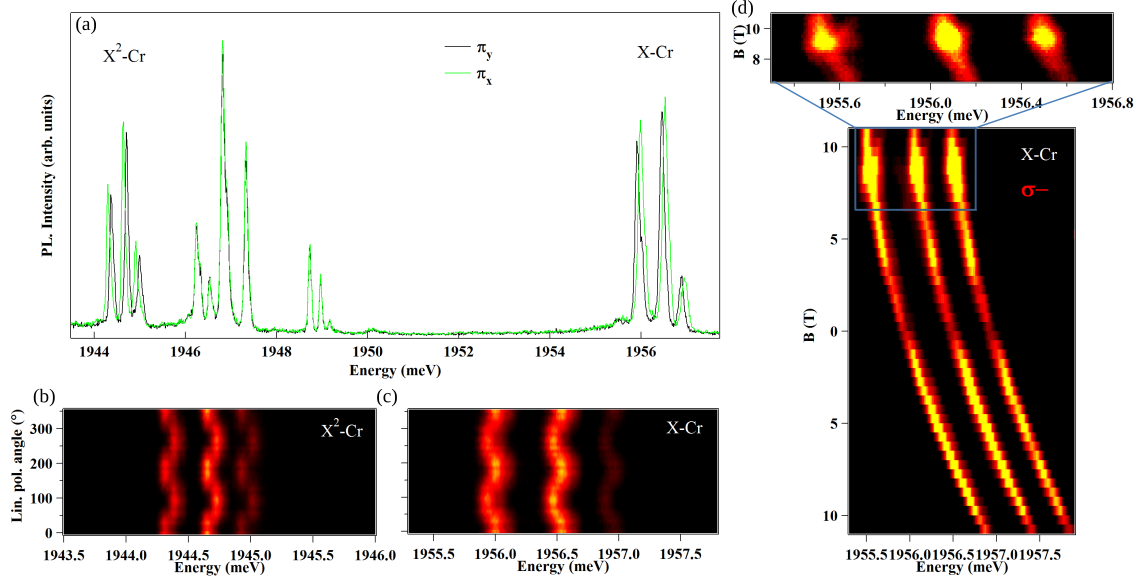
Figure II.12: (a) QD4 linearly polarized PL intensity at zero magnetic field. (b) and (c) Respectively X^2-Cr and X-Cr linear polarization PL dependence at zero magnetic of this QD. Both central and exterior peaks present linear polarization dependencies in this dots. (c) X-Cr magnetic field PL dependence on this QD. Zoom in presents anti-crossing appearing at B=9T.

that the overlap between the electron and the hole wave functions is changed by the application of an exterior electric field, to the point where they don't overlap at all.

Fig. II.14 shows that, using electric field, we can manipulate the splitting of any given charged state of the QD. For all positive bias voltage between 0V and 13V, X-Cr present a broad emission containing all six peaks in linear emission, as show on Fig. II.14(a). The emission then divide into three distinct peaks, starting to appear around -1V. This is evidenced on the the PL emission on Fig. II.14(d).

This three peaks emission structure looks like a three levels system emitting at three different energies. However, the magnetic field evolution presented in Fig. II.12(c) does not reflect the presence of a magnetic atom in the quantum dot. Moreover, evolution under electric field shows huge changes in the carriers wave functions overlap. These features hint for a single exciton trapped in the QD, presenting spectral fluctuations.

Spectral fluctuations under a fluctuation of charge in the vicinity of a QD has been observed to lead to a peak broadening [36], such as observed on Fig. II.14(d), as well as spectrum jumps. For the PL to jump between three emission energies,
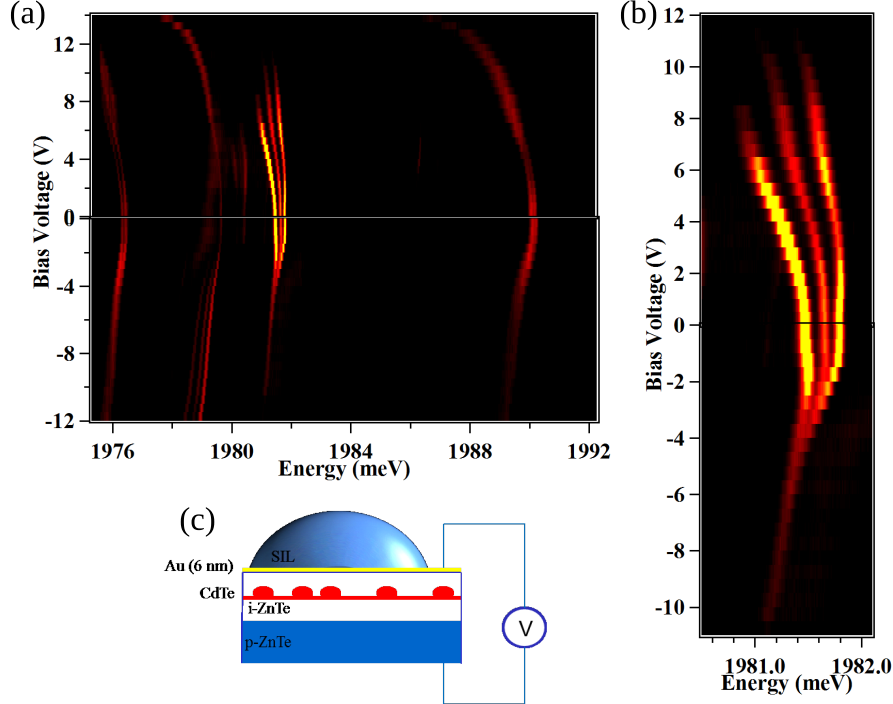
Figure II.13: (a) QD5 whole PL evolution under application of a bias voltage. (b) Zoom on X^c-Cr circular polarization PL intensity evolution under electric field. A strong stark shift is observed, as well as variation in the splitting. (c) Schema of the Schottky gate used to apply the bias voltage on the sample.

the charge fluctuation has to be able to take three distinct charge values.

Cr in ZnTe is incorporated as Cr^{2+}, but, as shown on Fig.II.15(a), the Cr$^+$ and Cr^{3+} are also accessible [37], either by capturing an electron (Cr$^+$) or a hole (Cr^{3+}). Considering such a charge close to the QD, it can be viewed as a punctual one, since the dot is far bigger than the atom. The effect on the wave functions, presented in Fig.II.15(b)-(d), differs depending on the electrical charge of the Cr atom. The electron is well confined in CdTe/ZnTe quantum dots, while the hole is almost not confined. Because of this, the electron wave function is almost not moved by the presence of the electric, when the hole one vary more depending on the charge state of the Cr. These differences in the overlapping of wave functions lead to three different emission energies depending on the Cr charge state.

The charge variation of the Cr is of the value of the elementary charge. Considering a pure coulomb interaction between two punctual charges, for a charge at 5nm of the dot, its effect is one order of magnitude below the confinement energy.
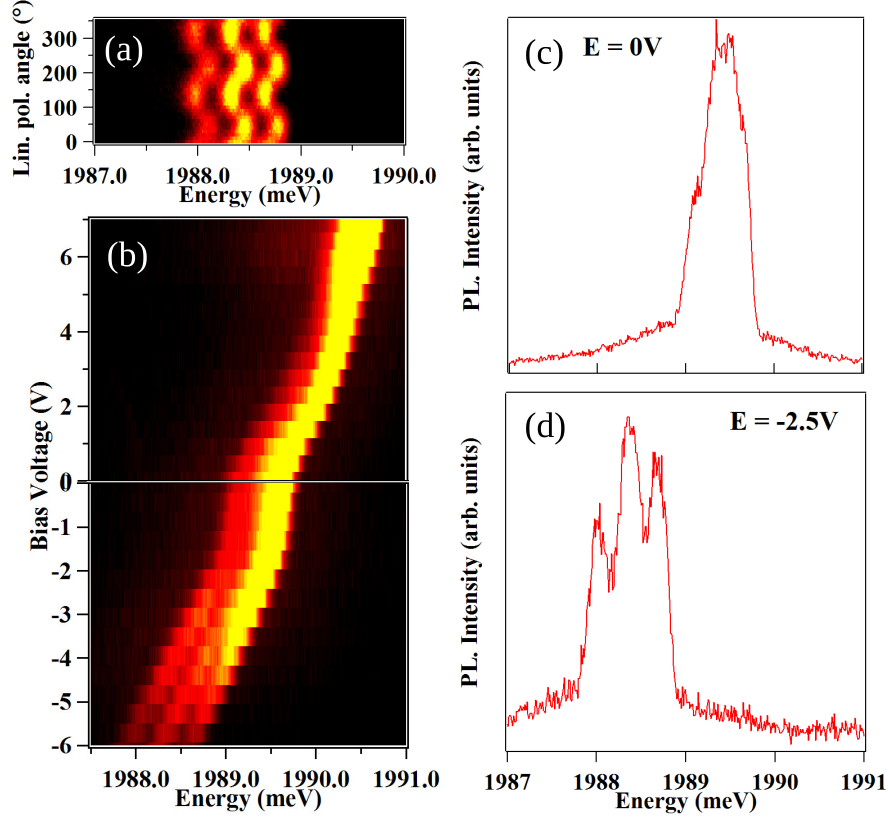
48

Figure II.14: All these measures were taken on QD6 X-Cr complex at low temperature. (a) PL intensity dependency in linear polarization. In order to have the best contrast, the map was taken at -2.5V bias voltage. (b) Circular PL intensity evolution in electric field. A splitting began to appear around -2V of applied bias voltage. (c)-(d) Circular PL for an applied bias voltage of, respectively, 0V and -2.5V.

In order to have a significant effect on the dot PL, the Cr has then to be close to it, not more than a few nanometres away.

This hypothesis is currently tested, along with the capacity for the Cr to diffuse outside the quantum dots layer.

II.4 Conclusion

For the first time, a single Cr atom in a semiconductor was probed optically. The fine structure of the Cr is dominated by a magnetic anisotropy induced by strain in the plane of the QDs. The large spin to strain coupling of Cr, two orders
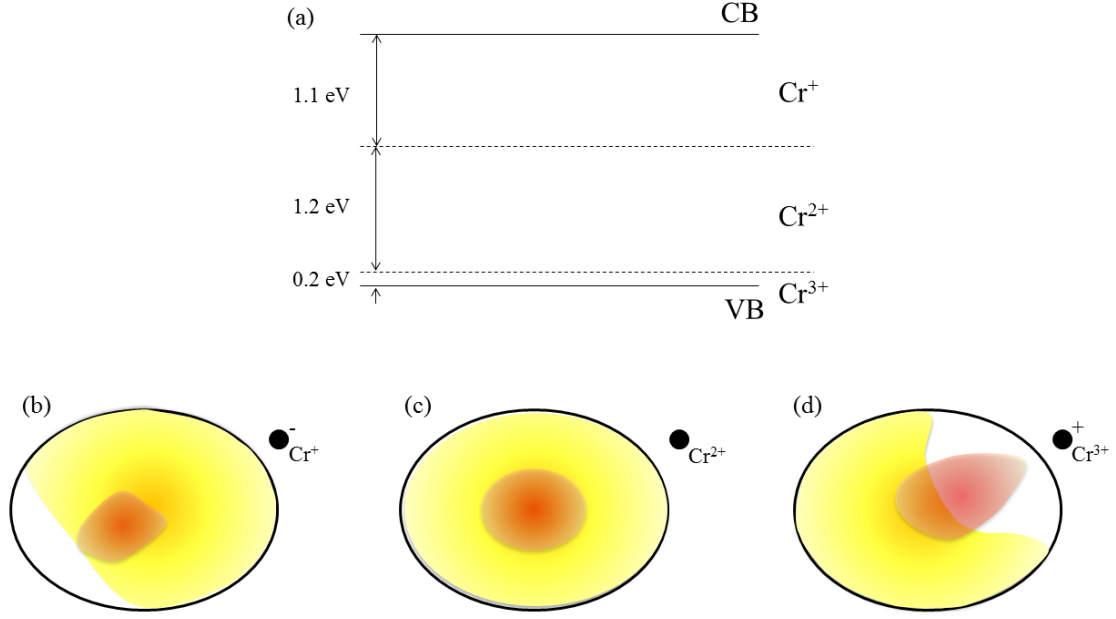
Figure II.15: (a) Cr accessible charged states in ZnTe. (b)-(d) Illustration of the effect of a punctual charge on the wavefunction of an electron (red) and a hole (yellow) in a quantum dots.

of magnitude larger than for magnetic elements without orbital momentum (NV centers in diamond [38], Mn atoms in II-VI semiconductors [39]) suggests some possible development of coherent mechanical spin-driving of an individual magnetic atom in a nano-mechanical oscillator. This new single spin system should allow, at low temperature, to enter some coupling regimes dominated by quantum coherent dynamics not reached until now in hybrid spin-mechanical devices.

Some dots presents the same structure at 0T than dots containing a single Cr atom, but without presenting the signature of the presence of a magnetic atom under magnetic field. These dots are effected by the variation of charge of a single Cr atom in the barrier, close to the dot. Further study of the diffusion process of Cr in CdTe and ZnTe is required in order to avoid the creation of such dots.

Bibliography

[1] E. O. Kane, "Band structure of indium antimonide", Journal of Physics and Chemistry of Solids **1**, 249–261 (1957).

[2] C. Le Gall, "Dynamics and Optical contrôl of a single spin in a Quantum Dot", Theses (Université de Grenoble, Nov. 2011).

[3] J. M. Luttinger, "Quantum theory of cyclotron resonance in semiconductors: general theory", Phys. Rev. **102**, 1030–1041 (1956).

[4] G. Bir and G. Pikus, *Symmetry and strain-induced effects in semiconductors*, Wiley (1974).

[5] J. Allègre, B. Gil, J. Calatayud, and H. Mathieu, "Deformation potentials of cdte epilayers from piezo and wavelength modulation reflectivity spectra analysis", Journal of Crystal Growth **101**, 603–607 (1990).

[6] J. M. Luttinger and W. Kohn, "Motion of electrons and holes in perturbed periodic fields", Phys. Rev. **97**, 869–883 (1955).

[7] J.-L. Basdevant and J. Dalibart, "Mécanique quantique", in (Les éditions de l'École Polytechnique, 2002) Chap. 2, p. 80.

[8] Y. Léger, "Détection de spins individuels dans les boîtes quantiques magnétiques", Theses (Université Joseph-Fourier - Grenoble I, Sept. 2007).

[9] Y. Léger, L. Besombes, L. Maingault, and H. Mariette, "Valence-band mixing in neutral, charged, and Mn-doped self-assembled quantum dots", Phys. Rev. B **76**, 045331 (2007).

[10] W. Wardzyński and M. Suffczyński, "Dependence of the exchange splitting in excitons on the interatomic distance", Solid State Communications **10**, 417–419 (1972).

[11] J. R. Schrieffer and P. A. Wolff, "Relation between the anderson and kondo hamiltonians", Phys. Rev. **149**, 491–492 (1966).

[12] L. Maingault, "Insertion d'ions magnétiques dans les boîtes quantiques de semi-conducteurs II-VI", Theses (Université Joseph-Fourier - Grenoble I, Dec. 2006).

[13] J. Gaj, R. Planel, and G. Fishman, "Relation of magneto-optical properties of free excitons to spin alignment of mn^2+ ions in cd$_{1-x}$mn$_x$te", Solid State Communications **29**, 435–438 (1979).

[14] P. Kacman, "Spin interactions in diluted magnetic semiconductors and magnetic semiconductor structures", Semicond. Sci. Technol. **16**, R25 (2001).

[15] W. Mac, A. Twardowski, and M. Demianiuk, "S,p-d exchange interaction in Cr-based diluted magnetic semiconductors", Phys. Rev. B **54**, 5528–5535 (1996).

[16] J. Blinowski, P. Kacman, and K. Majewski, "Ferromagnetism in cr-based diluted magnetic semiconductors", Journal of Crystal Growth **159**, Proceedings of the seventh international conference on II-VI compouds and devices, 972–975 (1996).

[17] M. Herbich, W. Mac, A. Twardowski, K. Ando, Y. Shapira, and M. Demianiuk, "Magnetization and exciton spectroscopy of the diluted magnetic semiconductor cd$_{1-x}$cr$_x$s", Phys. Rev. B **58**, 1912–1921 (1998).

[18] M. Zieli ński, Y. Don, and D. Gershoni, "Atomistic theory of dark excitons in self-assembled quantum dots of reduced symmetry", Phys. Rev. B **91**, 085403 (2015).

[19] J. T. Vallin and G. D. Watkins, "Epr of Cr^{2+} in II-VI lattices", Phys. Rev. B **9**, 2051–2072 (1974).

[20] J. T. Vallin and G. D. Watkins, "Epr of cr^{2+} in ii-vi lattices", Phys. Rev. B **9**, 2051–2072 (1974).

[21] M. Brousseau, *Les defauts ponctuels dans les semiconducteurs* (Les Editions de Physiques, Sept. 1988).

[22] R. D. Greenough and S. B. Palmer, "The elastic constants and thermal expansion of single-crystal CdTe", Journal of Physics D: Applied Physics **6**, 587 (1973).

[23] P. Ovartchaiyapong, K. W. Lee, B. A. Myers, and A. C. B. Jayich, "Dynamic strain-mediated coupling of a single diamond spin to a mechanical resonator", Nature Communications **5**, 4429 (2014).

[24] W. Mac, A. Twardowski, and M. Demianiuk, "S,p-d exchange interaction in Cr-based diluted magnetic semiconductors", Phys. Rev. B **54**, 5528–5535 (1996).

[25] M. Herbich, W. Mac, A. Twardowski, K. Ando, Y. Shapira, and M. Demianiuk, "Magnetization and exciton spectroscopy of the diluted magnetic semiconductor $Cd_{1-x}Cr_xS$", Phys. Rev. B **58**, 1912–1921 (1998).

[26] T. Takagahara, "Theory of exciton doublet structures and polarization relaxation in single quantum dots", Phys. Rev. B **62**, 16840–16855 (2000).

[27] J. McFarlane, P. A. Dalgarno, B. D. Gerardot, R. H. Hadfield, R. J. Warburton, K. Karrai, A. Badolato, and P. M. Petroff, "Gigahertz bandwidth electrical control over a dark exciton-based memory bit in a single quantum dot", Applied Physics Letters **94**, 093113 (2009).

[28] M. Bayer, G. Ortner, O. Stern, A. Kuther, A. A. Gorbunov, A. Forchel, P. Hawrylak, S. Fafard, K. Hinzer, T. L. Reinecke, S. N. Walck, J. P. Reithmaier, F. Klopf, and F. Schäfer, "Fine structure of neutral and charged excitons in self-assembled In(Ga)As/(Al)GaAs quantum dots", Phys. Rev. B **65**, 195315 (2002).

[29] D. Gammon, E. S. Snow, B. V. Shanabrook, D. S. Katzer, and D. Park, "Fine structure splitting in the optical spectra of single GaAs quantum dots", Phys. Rev. Lett. **76**, 3005–3008 (1996).

[30] L. Besombes and H. Boukari, "Resonant optical pumping of a Mn spin in a strain-free quantum dot", Phys. Rev. B **89**, 085315 (2014).

[31] Y. Léger, L. Besombes, L. Maingault, D. Ferrand, and H. Mariette, "Geometrical effects on the optical properties of quantum dots doped with a single magnetic atom", Phys. Rev. Lett. **95**, 047403 (2005).

[32] M. Zieli ński, Y. Don, and D. Gershoni, "Atomistic theory of dark excitons in self-assembled quantum dots of reduced symmetry", Phys. Rev. B **91**, 085403 (2015).

[33] L. Besombes, Y. Leger, L. Maingault, D. Ferrand, H. Mariette, and J. Cibert, "Carrier-induced spin splitting of an individual magnetic atom embedded in a quantum dot", Phys. Rev. B **71**, 161307 (2005).

[34] A. H. Trojnar, M. Korkusinski, U. C. Mendes, M. Goryca, M. Koperski, T. Smolenski, P. Kossacki, P. Wojnar, and P. Hawrylak, "Fine structure of a biexciton in a single quantum dot with a magnetic impurity", Phys. Rev. B **87**, 205311 (2013).

[35] B. Varghese, H. Boukari, and L. Besombes, "Dynamics of a Mn spin coupled to a single hole confined in a quantum dot", Phys. Rev. B **90**, 115307 (2014).

[36] H. Kamada and T. Kutsuwa, "Broadening of single quantum dot exciton luminescence spectra due to interaction with randomly fluctuating environmental charges", Phys. Rev. B **78**, 155324 (2008).

[37] J. Dziesiaty, P. Peka, M. U. Lehr, A. Klimakow, S. Müller, and H.-J. Schulz, "The chromium impurity in znte: changes of the charge state detected by optical and EPR spectroscopy", ZPCH **201**, 63 (1997).

[38] A. Barfuss, J. Teissier, E. Neu, A. Nunnenkamp, and P. Maletinsky, "Strong mechanical driving of a single electron spin", Nat Phys **11**, 820 (2015).

[39] A. Lafuente-Sampietro, H. Boukari, and L. Besombes, "Strain-induced coherent dynamics of coupled carriers and Mn spins in a quantum dot", Phys. Rev. B **92**, 081305 (2015).